UNIVERSITY OF OKLAHOMA

GRADUATE COLLEGE

SULFIDE STRESS CRACKING BEHAVIOR OF GRADE C-110, Q-125 AND T-95 STEEL TUBULARS UNDER HIGH-PRESSURE CONDITIONS

A THESIS

SUBMITTED TO THE GRADUATE FACULTY

in partial fulfillment of the requirements for the

Degree of

MASTER OF SCIENCE

By

JIWON JEON
Norman, Oklahoma
2016

Downloaded from SHAREOK. Persistent Handle URL: https://hdl.handle.net/11244/47099

SULFIDE STRESS CRACKING BEHAVIOR OF GRADE C-110, Q-125 AND T-95 STEEL TUBULARS UNDER HIGH-PRESSURE CONDITIONS

A THESIS APPROVED FOR THE
MEWBOURNE SCHOOL OF PETROLEUM AND GEOLOGICAL ENGINEERING

BY

_____
Dr. Ramadan Ahmed, Chair

_____
Dr. Catalin Teodoriu

_____
Dr. Saeed Salehi

© Copyright by JIWON JEON 2016
All Rights Reserved.

This thesis is dedicated to my parents, my sister, and my brother.

ACKNOWLEDGEMENTS

I appreciate all those who have supported me to complete this research and thesis successfully. This thesis is not only my work in the lab, but also it is priceless experience that I have gained through the school years. I could not have achieved this without the help and encouragement of everyone.

First and foremost I would like to express my deepest gratitude to my advisor, Dr. Ramadan Ahmed. He provided me with a great opportunity to work on this project and has always been supportive, for allowing me to cultivate academic knowledge and passion. His unstinting guidance and constructive feedback improved my research ability and professional skills.

I also would like to thank my committee members, Dr. Catalin Teodoriu and Dr. Saeed Salehi, for their valuable time and inputs to my research. Thanks to their advice, I was able to learn the subject in depth. I am also grateful to Dr. Subhashi Shah for his contribution to establish a wonderful research environment for the experiment.

Furthermore, I sincerely appreciate Mr. Jeff McCaskill for his tremendous help for the experimental tests. The laboratory investigation would have been impossible without him as he always gave the solutions to any mechanical problems. I also thank my research mates, Rida Elgaddafi, Sagar Tale, Omotayo Omosebi and Tarek Firoze for their help to have interesting discussion on the experiment. I would like to express my special thanks to Ankita Sinha, Sama Khosravi, Yuji Kim, Dongho Jo, Ayoung Jo, WCTC members and all of my friends for their encouragement.

Lastly, I convey my love and gratitude to my family for their constant support.

TABLE OF CONTENTS

ACKNOWLEDGEMENTS ..... **iv**

TABLE OF CONTENTS ..... **v**

LIST OF TABLES ..... **viii**

LIST OF FIGURES ..... **ix**

ABSTRACT ..... **xii**

CHAPTER 1 : INTRODUCTION **1**

1.1 Overview 1

1.2 Statement of the Problem 2

1.3 Objectives 3

1.4 Scope of Work 4

CHAPTER 2 : LITERATURE SURVEY **7**

2.1 Corrosions on Downhole Tubulars 7

2.2 Mechanism of Sulfide Stress Cracking (SSC) 8

2.3 Factors Affecting SSC Resistance 11

2.3.1 pH and H_2S partial pressure 11

2.3.2 Temperature 13

2.3.3 Metallurgical Properties 13

2.4 SSC Measurement 15

2.4.1 NACE Method A – Tensile Test 16

2.4.2 Slow Strain Rate Test 17

2.5 Stress – Strain Prediction from Tensile Test 19

2.5.1 Elastic Deformation 22

2.5.2 Uniformly Plastic Deformation 22

2.5.3 Non-uniform Plastic Deformation after Necking 24

CHAPTER 3 : EXPERIMENTAL STUDY 29

3.1 Measuring Strategy 29

3.2 Test Materials 30

3.3 Test Apparatuses Used During the Investigation 32

3.3.1 TST Apparatus 32

3.3.2 SSC Test Schematic 34

3.3.3 SSC Cell 36

3.4 Test Conditions 38

3.5 Test Procedure 41

CHAPTER 4 : DATA ANALYSIS AND INTERPRETATION 46

4.1 Mechanical Properties 46

4.2 Failure Analysis 49

4.2.1 Stress – Strain Profile 49

4.2.2 Crack Features 60

4.3 Effect of CO_2 66

CHAPTER 5 : CONCLUSIONS AND RECOMMENDATIONS 74

5.1 Conclusions 74

5.2 Recommendations 75

NOMENCLATURE 76

REFERENCES..... 77

LIST OF TABLES

Table 2.1: Dimensions of Method A test specimens 16

Table 3.1: Chemical compositions of tested carbon steels 31

Table 3.2: Dimensions of test specimen* 31

Table 3.3: Hydraulic pressure required for TST test 39

Table 3.4: Testing conditions for SSC experiment 40

Table 4.1: Mechanical properties of T-95 specimens after SSC test 48

Table 4.2: Mechanical properties of C-110 specimens after SSC test 48

Table 4.3: Mechanical properties of Q-125 specimens after SSC test 49

Table 4.4: Typical chemical compositions of API carbon steels 71

LIST OF FIGURES

Figure 1.1: Conditions of casing exposure to sour gas (Rhodes et al. 2007)..... 3

Figure 1.2: Regions of environmental severity with respect to the SSC of carbon and low-alloy steels (NACE Standard 2009)..... 5

Figure 2.1: Schematic of hydrogen generation producing SSC (NACE Standard 2009)..... 9

Figure 2.2: Schematic of SCC mechanism (Heidary et al. 2008)..... 10

Figure 2.3: SSC failure windows for pH and H_2S partial pressure (Tale (2014) redrawing from Morana and Nice (2009)): a) P-110; b) Q-125; c) Grade 140; and d) Grade 150 12

Figure 2.4: Threshold stress vs. Hardness (Tale (2014) redrawing from Ciaraldi (1986))..... 14

Figure 2.5: Schematic of Method A test specimens (NACE Standard 2009)..... 16

Figure 2.6: Comparison chart between Method A result and CERT EpR :(a) Dependence of CERT parameter of C-110 materials on normalized time-to-failure of Method A; and (b) Correlation of EpR to average time-to- failure of Method A for C-110 (Hörstemeier et al. 2010) 18

Figure 2.7: Engineering stress-strain curve for ductile steel 20

Figure 2.8: Necking geometry used in Bridgman correction method (Ling 1996) 26

Figure 3.1: Test specimen: a) without adapters; and b) with adapters..... 32

Figure 3.2: TST apparatus: a) schematic; and b) picture..... 33

Figure 3.3: SSC test schematic..... 34

Figure 3.4: SSC Cell: a) Schematic; and b) Side view of specimen gauge section..... 38

Figure 4.1: 0.2% offset yield strength measurement for T-95 baseline specimen..... 47

Figure 4.2: Stress-Strain profiles: a) C-110-1; and b) C-110-2 (baseline) 50

Figure 4.3: Stress-strain profiles: a) T-95-1 (baseline); and b) T-95-2..... 50

Figure 4.4: Stress-strain profiles: a) Q-125-1 (baseline); and b) Q-125-2..... 51

Figure 4.5: Stress-strain profiles of limit test specimens: a) T-95-5; b) C-110-5; and c) Q-125-5 51

Figure 4.6: Stress-Strain profiles: a) T-95-3; b) C-110-3; and c) Q-125-3 52

Figure 4.7: Stress-strain profiles of specimens exposed to corrosive environment containing 2.5% CO_2: a) T-95-4; b) C-110-4; and c) Q-125-4 53

Figure 4.8: Stress-strain profiles of specimens exposed to corrosive environment containing 5% CO_2: a) T-95-5; b) C-110-5; and c) Q-125- 5 54

Figure 4.9: Stress-strain profiles of specimens exposed to corrosive environment containing 10% CO_2: a) T-95-6; and b) Q-125-6 55

Figure 4.10: Schematic of failure of specimens exposed to corrosive environment containing 10% CO_2: a) Front view of T-95-6; b) Microscopic view of T-95-6; c) Front view of Q-125-6; and d) Microscopic view of Q-125-6 56

Figure 4.11: Stress-strain profiles of specimens exposed to corrosive environment containing 15% CO_2: a) T-95-7; b) C-110-9; c) C-110-10; and d) Q-125-7 57

Figure 4.12: Stress–strain profiles of specimens exposed to corrosive environment containing 25% CO_2: a) T-95-8; b) T-95-9; c) C-110-11; d) C-110-12; and e) Q-125-9 58

Figure 4.13: Stress–strain profiles of specimens exposed to corrosive environment containing 40% CO_2: a) T-95-10; b) C-110-13; and c) Q-125-10 59

Figure 4.14: Crack features of baseline specimens: a) T-95-1; b) C-110-2; and c) Q-125-1 60

Figure 4.15: Crack features of specimens used in pressure holding tests: a) T-95-2; b) C-110-1; and c) Q-125-2 61

Figure 4.16: Crack features of specimens exposed to the corrosion environment in absence of CO_2: a) T-95-3; b) C-110-3; and c) Q-125-3 61

Figure 4.17: Crack features of specimens exposed to the corrosion environment containing 2.5% CO_2: a) T-95-4; b) C-110-4; and c) Q-125-4 62

Figure 4.18: Crack features of specimens exposed to the corrosion environment containing 5% CO_2: a) T-95-5; b) C-110-5; and c) Q-125-5 62

Figure 4.19: Comparison of features of brittle and ductile failures: a) Q-125-5; and b) Q-125-1 (baseline) 63
Figure 4.20: Crack features of specimens exposed to the corrosive environment containing 10% CO_2 concentration: a) T-95-6; and b) Q-125-6 63
Figure 4.21: Crack features of C-110 specimens exposed to the corrosive environment containing 10% CO_2 concentration: a) C-110-6; b) C-110-7; and c) C-110-8 64
Figure 4.22: Crack features of specimens exposed to the corrosive environment containing 15% CO_2 concentration: a) T-95-7; b) C-110-9; c) C-110-10 (repeated test); and d) Q-125-5 64
Figure 4.23: Crack features of specimens exposed to the corrosive environment containing 25% CO_2 concentration: a) T-95-8; b) T-95-9; c) C-110-11;d) C-110-12; e) Q-125-8; and f) Q-125-9 65
Figure 4.24: Crack features of specimens exposed to the corrosive environment containing 40% CO_2 concentration: a) T-95-10; b) C-110-13; c) C-110-14; and d) Q-125-10 66
Figure 4.25: Ultimate tensile strength vs. CO_2 concentration: a) T-95; b) C-110; and c) Q-12567
Figure 4.26: Plastic strain to failure vs. CO_2 concentration: a) T-95; b) C-110; and c) Q-125 .. 69
Figure 4.27: Ultimate tensile strength vs. CO_2 concentration 70
Figure 4.28: Plastic strain to failure vs. CO_2 concentration 71
Figure 4.29: Dimensionless Ultimate tensile strength vs. CO_2 concentration 72
Figure 4.30: Normalized Plastic strain to failure vs. CO_2 concentration 73

ABSTRACT

Due to the expansion of hydrocarbon exploration into challenging sour oil and gas resources, the industry is now facing severe sour related corrosion problem. Sulfide Stress Cracking (SSC) is one of the detrimental types of corrosion which happens in sour environment. SSC quickly diminishes performance of downhole tubulars. The embrittlement induced by SSC causes failure of steel at a stress level, which is significantly lower than its yield strength. A premature failure of downhole tubulars impacts safety and operational issues during drilling, completion and production phases. Therefore, it is necessary to study the failure behavior of carbon steels used in sour environment.

The principal aim of this study is to understand mechanisms of SSC in the presence of CO_2 and experimentally investigate the failure characteristics of API steels (T-95, C-110 and Q-125) exposed to high-pressure sour environment while subjected to a tensile load. Hence, to carry out the experimental investigation, minipipe specimens were cut and manufactured from API grade tubulars. During the test, a specimen was place in a SSC test cell (high-pressure autoclave), which was partially filled with 2% NaCl solution saturated with mixed gas containing CH_4, CO_2 and H_2S. In the cell, the specimen was strained to create stress level, which is equal to 80% of its yield strength while maintaining the desired CH_4, CO_2 and H_2S partial pressures for seven days to simulate the corrosive environment. The total pressure inside the specimen was kept at 6,000 psi while the outer pressure was held at 4,000 psi.

Impact of CO_2 content of the gas phase on SSC is examined varying CO_2 concentration (i.e. ratio of partial pressure of CO_2 to the total pressure) from 0 to 40%.

All tests were conducted at constant temperature (100°F) and H_2S concentration (300 ppm). Temperature of 100°F is chosen for the CO_2 investigation because SSC is known to occur at low temperature causing considerable change in mechanical properties of steel. Mechanical property changes occurring after exposure to the corrosive environment is used to quantify embrittlement of test specimens. Hence, mechanical properties of the specimens were measured after the exposure using Tensile Strength Testing (TST) apparatus and compared to the initial mechanical properties of an uncorroded clean specimen (baseline). After strength testing, microscopic examination was performed on broken specimens to assess embrittlement of the specimens based on crack features and shear deformation pattern.

According to the experimental results, SSC susceptibility of T-95 and C-110 grade steels is maximized at about 10% CO_2 while that of Q-125 grade maximized at 25% CO_2. The experiment reveals that tested carbon steels are safe to use without SSC concerns in environment containing H_2S content of up to 300 ppm which is equivalent to 1.8 psi at total pressure of 6000 psi. However, presence of CO_2 in sour environment significantly reduces the SSC resistance of steel especially when CO_2 concentration is in the range of 10 to 30%.

CHAPTER 1: INTRODUCTION

1.1 Overview

During hydrocarbon exploration and production, tubulars including drill pipe, casing and tubing, are exposed to a variety of corrosive environment. The major functions of the tubulars are transportation of downhole fluids and maintain integrity of the wells and their vicinity. Hence, corrosion of tubulars is a major problem in maintaining drilling and production performance and safety. In addition to the common corrosion problem induced by formation water, existence of corrosive gases such as carbon dioxide (CO_2) and hydrogen sulfide (H_2S) exacerbates the problem.

When H_2S is present in the system, it is called "sour" environment. H_2S itself does not have serious corrosive behavior; however, it becomes a corrosive agent in contact with aqueous environment, in which an exposed metal reacts with dissolved H_2S gas (Popoola et al. 2013).

$$Fe + H_2S + H_2O \rightarrow FeS + 2H + H_2O \quad (1.1)$$

H_2S not only serves as a reactant, but also acts as a catalyst for both anodic and cathodic reactions occurring during corrosion process. Sour corrosion generally results in uniform, pitting, and stepwise cracking. Sulfide stress cracking (SSC) is also one of the common types of localized corrosion occurring in sour environment when tubulars are subject to loading condition depending on the application. (Ciaraldi 1986) Common examples of loading conditions that tubulars can be exposed during service life:

- Drill pipe rotates the bit and circulates drilling fluid with cuttings. It is subject

to axial tensile load by its weight, internal pressure occurred by drilling fluid, and additionally bending loads if directional drilling is applied.

- Casing is also under axial tension by its dead weight and fluid pressure, in addition to external pressure by surrounding formation.
- Production tubing is highly affected by the fluid purging pressure as well as the axial tensile load.

SSC is of importance to investigate since it degrades tubulars by embrittlement process resulting in early fracture of the pipes at a stress level well below yield strength. Several factors affecting SSC are presented in Chapter 2 and the influence of CO_2 concentration on SSC is analyzed and discussed in Chapter 4 along with experimental results.

1.2 Statement of the Problem

As discussed in Section 1.1, downhole tubulars in sour environment are often under loading condition, which leads to SSC embrittlement and subsequent failure. Small amount of H_2S is sufficient to initiate the corrosion process and certain level of CO_2 concentration accelerates the degradation process. As a result, SSC embrittlement occurs quickly causing premature failure, which is especially dangerous in terms of sour gas leakage to the surrounding environment. A gas leak may cause serious pollution of the groundwater and threat to the well safety during exploration and production. Figure 1.1 displays the leaking mechanism induced by the production casing failure, which depicts the problematic situation in total tubular system.

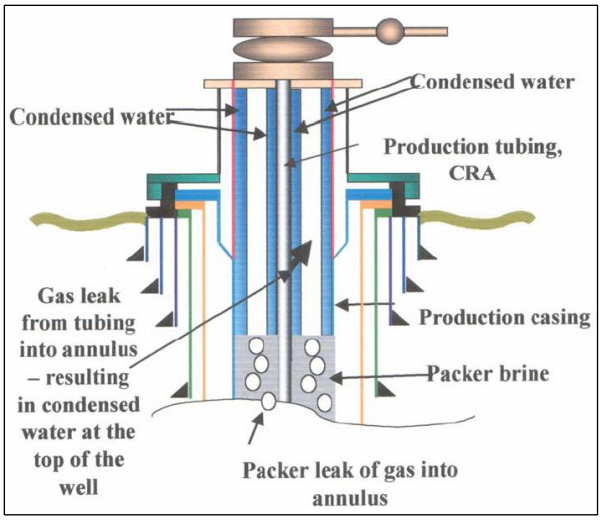


Figure 1.1: Conditions of casing exposure to sour gas (Rhodes et al. 2007)

Often unexpected rupture of metallic tubulars in oil and gas wells are associated with the exposure to H_2S containing downhole fluids. Hence, it is required to evaluate performance of standard materials that can be employed in such environment and identify the governing factors that determine the optimal operating conditions of the well.

1.3 Objectives

In order to mitigate the detrimental effect of SSC described in the previous sections, this research focuses on investigating the corrosion occurring in downhole by simulating the actual exploration and production environments in the lab. The main objectives of this study are:

- To understand the overall mechanism of H_2S involved corrosion under tensile loading conditions;
- To determine the factors affecting the SSC susceptibility of metallic tubulars;

- To experimentally evaluate the influence of CO_2 concentrations on SSC susceptibility of API tubulars (T-95, C-110 and Q-125) under sour condition; and
- To study the effect of CO_2 concentration on SSC of the API tubulars.

1.4 Scope of Work

This study includes literature review and experimental study. Literature review is conducted to provide the background theory and understand mechanical characteristics of carbon steels that susceptible for SSC failure. After studying mechanical properties of the selected steels (C-110, Q-125 and T-95), a test matrix for SSC experiment has been developed based on modeling results of Tale (2014), which estimated the required test duration and SSC susceptibility of API grade steels under different experimental conditions. Controlling variables for the experiment are CO_2 concentration and different types of steel grade. H_2S presence in the system was also evaluated by applying a fixed partial pressure of H_2S. In order to assess mechanical degradation of the API steels, SSC experiments were conducted under constant pressure and tensile load conditions. Mechanical properties of the selected API steels were measured after exposure to the corrosive environment, which simulates the downhole condition. The differences between mechanical properties of exposed and unexposed (baseline) minipipe specimen are used to quantify the embrittlement resulted due to SSC corrosion.

Test procedure is adopted from National Association of Corrosion Engineers (NACE) Method A (tensile test). This method requires testing duration of one month to enable reasonable SSC resistance evaluation; however, a modified method (integrating

NACE Method A and Constant Extension Stress Test) with shorter duration of testing time is implemented in this study to perform SSC experiments in a short time duration. Modified API Full Scale SSC Test using miniature hollow pipe was also applied to demonstrate tubular condition. Detailed description on test setups and procedures used in the investigation are presented in Chapter 3.

Even though literature review provides several factors such as tensile load, temperature, and H_2S partial pressure affecting the SSC, this study focuses on investigating the influence of CO_2 concentrations on SSC of different API steel grades. The concentrations of CO_2 and H_2S in the corrosion environment determines test fluid pH that can change the experimental condition into SSC regions defined by NACE standard. The severity of the sour environment with respect to the SSC is shown in Fig. 1.2.

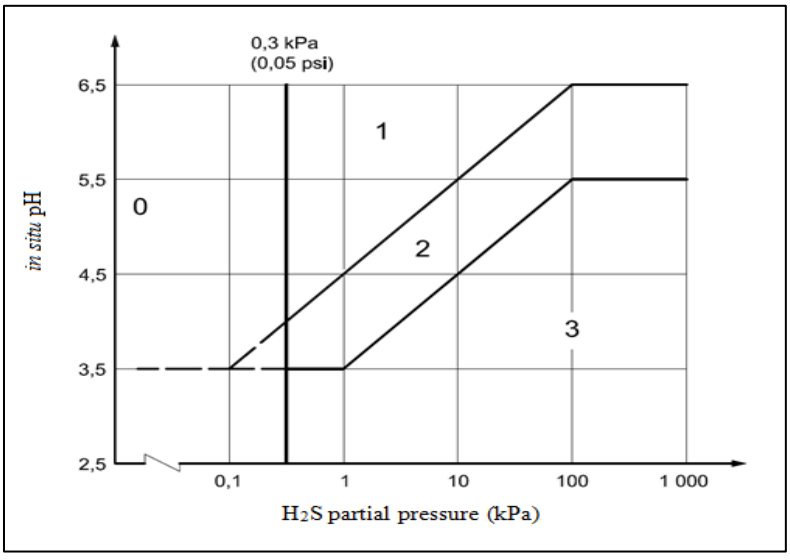


Figure 1.2: Regions of environmental severity with respect to the SSC of carbon and low-alloy steels (NACE Standard 2009)

The abbreviations used in Fig. 1.2 are denoted as below:

0: region 0, non-sour environment

1: SSC region 1, low severity sour environment

2: SSC region 2, moderate severity sour environment

3: SSC region 3, high severity sour environment

in situ pH: solution pH in the sour environment

The non-sour and sour environments are separated by 0.05 psi vertical line. The SSC experiments of T-95, C-110 and Q-125 covers three regions presented in Fig. 1.2, by varying the concentration of CO_2 and subsequently varying solution pH. NACE recommends relating solution pH to CO_2 partial pressure. In this study, H_2S partial pressure was maintained constant (300 ppm) while CO_2 partial pressure was varied from 0 psi to 2,400 psi, resulting in pH values ranging from 3 to 4. To simulate general downhole condition, 2% NaCl solution (brine) was used as aqueous phase. The brine used in the experiment is expected to minimize the solution connate pH effect. Testing results of SSC experiment of each steel grade are presented in Chapter 4.

CHAPTER 2: LITERATURE SURVEY

Sulfide stress cracking phenomenon has been extensively studied by a number of researchers in academic and industrial fields. (Bourgoyne et al. 1986; Ciaraldi 1986; Craiget al. 1992; Kimura et al. 1996; Vera and Case 1997; Hashizume and Inohara 2000; Koh et al. 2004; Cernocky et al. 2005; Morana and Nice 2009; Hörstemeier et al. 2010; Crowder et al. 2011; Papavinasam 2013) In this chapter, the mechanism of SSC along with the critical factors influencing SSC resistance are presented. Standard SSC testing methods and measurement techniques are briefly introduced. Moreover, theoretical and empirical approaches used to assess SSC by analyzing mechanical properties of tubulars after exposure to corrosive environment.

2.1 Corrosions on Downhole Tubulars

Corrosion is generally distinguished by the following taxonomy (Bell 2016);

- Uniform corrosion: the most common type of corrosion caused by electrochemical reaction which produces the deterioration of the entire material surface.
- Localized corrosion: the corrosion occurs only at certain area of the material surface. Three subclasses of localized corrosion are: pitting, crevice corrosion and filiform corrosion. Pitting happens due to a depassivation of a small area, forming a cavity which can further lead to failure of the metal. Crevice corrosion also occurs at a specific location similar to pitting. It is usually related to acidic condition or a depletion of oxygen in a crevice generally found under gaskets. Filiform corrosion is

associated with water breaching of the coating and painting, which leads to structural weakness.

- Galvanic corrosion: it involves two different metals acting either anode or cathode. The anodic metal experiences faster deterioration while the cathodic metal is protected by the anode and resulted in slow corrosion rate.
- Environmental cracking: the environmental surroundings such as temperature, stress and chemicals that the metal experiences can lead to defect of the material. Stress corrosion cracking, sulfide stress cracking, hydrogen embrittlement and corrosion fatigues usually classified as this type of corrosion.

Sulfide stress cracking (SSC) has now became a general occurrence in oil and gas production field as the tubulars are subject to heavier dead weight and suffer severe sour condition with H_2S as the exploration activities expand to deeper reservoirs. The following sections thoroughly describe the SSC.

2.2 Mechanism of Sulfide Stress Cracking (SSC)

Sulfide Stress Cracking (SSC) is a cracking process resulted from hydrogen embrittlement in presence of wet H_2S under tensile load. The result of SSC appears as a crack to failure at stress level below the yield strength of the material. Hydrogen ions are generated by the corrosion process, which later turns into atomic hydrogen by oxidizing the metal on the surface of material. These atomic hydrogen penetrates into the metal lattice structure resulting in material embrittlement and eventually failure at

stress level below its tensile strength. Figure 2.1 shows the process of creating SSC fracture in terms of hydrogen atom penetration.

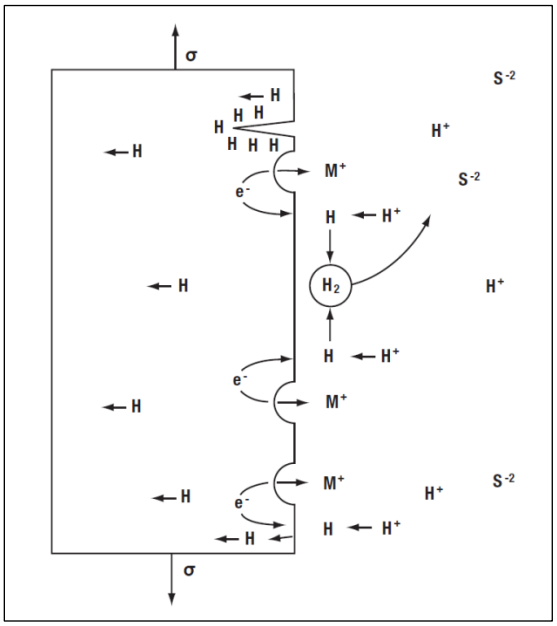


Figure 2.1: Schematic of hydrogen generation producing SSC (NACE Standard 2009)

SSC generally requires the following conditions to occur (Crowder et al. 2011):

- Sustained tensile load
- Presence of structural defect (usually carbon and low alloy steel)
- Hydrogen penetration into the metal supported by an aqueous sour environment with sufficient amount of H_2S: NACE defines H_2S concentration at least of 0.05 psi to promote SSC failure in 65 psi hydrocarbon gas.
- Temperature ranged from 20 to 120°F: temperature below 20°F causes too slow hydrogen diffusion rate, which never reaches the critical concentration for embrittlement. Meanwhile, temperature above 120°F

leads to too rapid diffusion of hydrogen atoms to stay and react with the metal lattice.

SSC is normally understood as a severe version of stress corrosion cracking (SCC) with specific corrosive agent (H_2S). However, SSC is associated with cathodic mechanism while SCC is a process of anodic dissolution. In SCC, the stress corrosion crack initiated by the rupture of brittle passive oxide film due to tensile load resulting in the exposure of metal surface to the corrosive environment. The clean metal surface goes through anodic dissolution of losing electrons to the surroundings. The corrosion creates new oxide film and the process of film-formation and rupturing repeats until the metal fails. Figure 2.2 presents the detailed schematic of SCC mechanism.

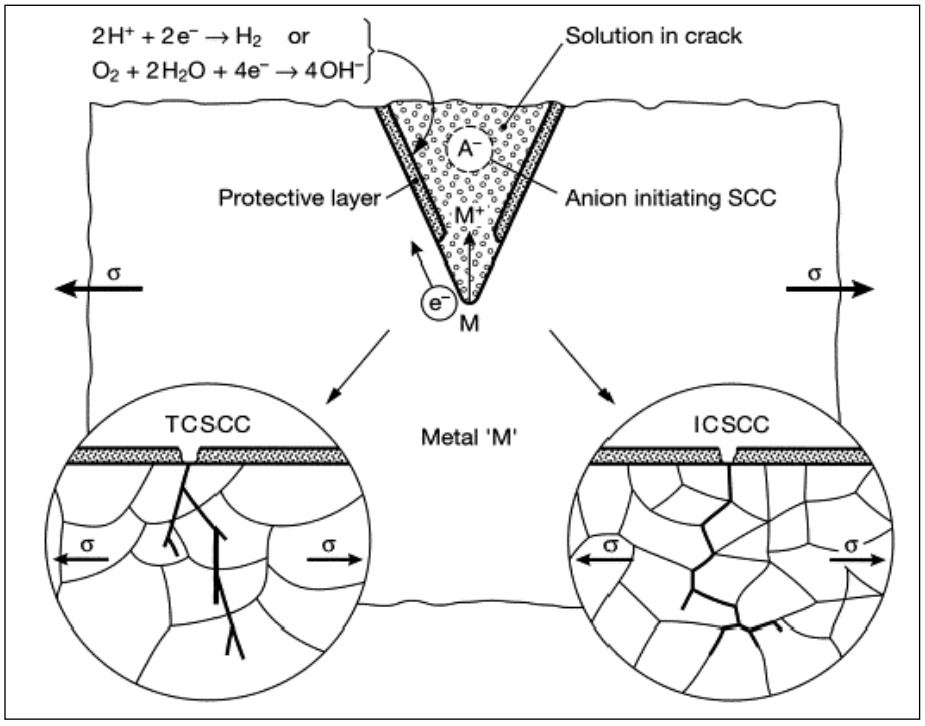


Figure 2.2: Schematic of SCC mechanism (Heidary et al. 2008)

SSC occurs in similar way as SCC. SSC mechanism involves the following reactions, which are facilitated by H_2S present in the solution:

$$M \rightarrow M^{+} + e^{-} \tag{2.1}$$

$$H^{+} + e^{-} \rightarrow H_{ads} \rightarrow H_2(g)$$

$$\rightarrow H_{diff} \tag{2.2}$$

where H_{ads}, atomic hydrogen adsorbed on the metal surface either proceeds to form hydrogen gas which bubbles from the surface or diffuses into the metal developing embrittlement. H_2S hinders the hydrogen gas (molecule) formation, promotes more hydrogen atoms to penetrate into the metallic lattice structure. (Papavinasam 2013)

2.3 Factors Affecting SSC Resistance

In this section, major environmental and metallurgical factors affecting the SSC susceptibility of steel tubulars are briefly described.

2.3.1 pH and H_2S partial pressure

Among numerous environmental influences, pH and H_2S partial pressure in the surrounding solution are considered to be the most critical factors that determine SSC resistance of a metal. Morana and Nice (2009) studied the SSC resistance of high-strength carbon steels (P-110, Q-125, Grade 140 and 150) by varying pH and H_2S partial pressure from 3.5 to 5.5 and 0.015 to 7.25 psi, respectively. NACE Method A was used to test the materials. The testing outcomes showed that P-110 survived for 25 hours with 7.25 psi of H_2S partial pressure at pH 5.5, while it lasted for entire 720 hours testing duration at lower H_2S partial pressures. As pH decreases from 5.5 to 3.5, SSC susceptibility of P-110 increases, failing at the lower H_2S partial pressures. Q-125 showed the same trend as P-110, however, failed at a milder sour conditions than that of P-110. Figure 2.3 display the SSC behavior of the tested specimens in terms of pH and H_2S partial pressure. It provides safety windows where the steel grades can be

used for downhole operation without concern of SSC failure. The overall results of the study indicated that SSC susceptibility of a metal increases with reduction in solution pH and increase in H_2S concentration. It was also concluded that steel grades with higher yield strength have higher susceptibility to SSC.

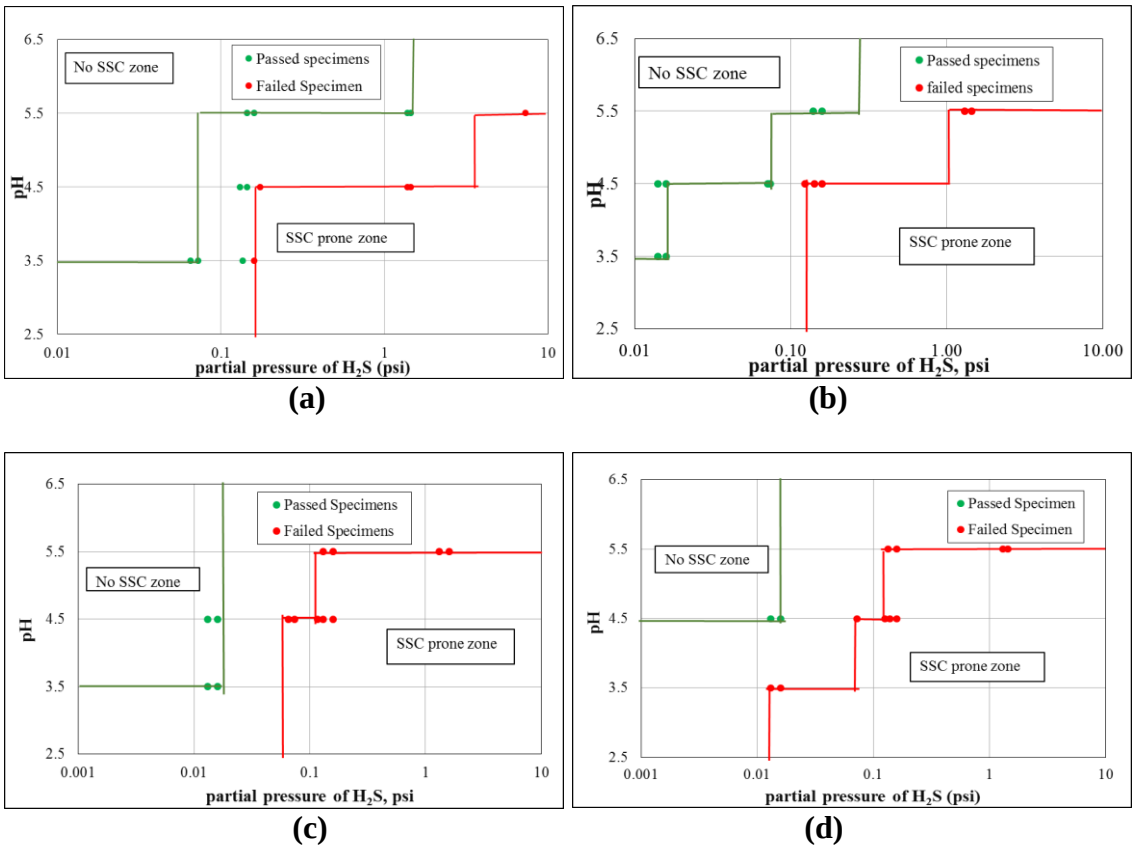


Figure 2.3: SSC failure windows for pH and H_2S partial pressure (Tale (2014) redrawing from Morana and Nice (2009)): a) P-110; b) Q-125; c) Grade 140; and d) Grade 150

Hashizume and Inohara (2000) also tested the effect of pH at a constant H_2S partial pressure by applying a constant level of tensile load, which develops stress level of 90% of yield strength of the specimen material. From the experiment, specimen showed considerable improvement in SSC resistance with increasing pH. Researchers

also revealed the depassivation pH at which corrosion rate of the metallic specimen drastically reduced, providing safe operation condition without causing SSC problem.

2.3.2 Temperature

Temperature of the surrounding corrosion environment is another major factor that strongly affects the SSC resistance of a metal. Vera and Case (1997) studied the effect of temperature by varying temperature from 77 to 203°F at pH 2.5. The experiments were performed by using Double Cantilever Beam (DCB) test, and the critical stress intensity factor (K_{ISSC}) was measured to compare the SSC resistance. The critical stress intensity factor is a parameter that shows the threshold value of stress state (intensity) required to propagate the crack. The result showed that the SSC resistance was improved from 19.6±1.4 to 34.4±2.4 Mpa* $m^{0.5}$ of K_{ISSC} values with temperature increase from 77 to 203°F. Bourgoyne et al. (1986) also explained that the carbon steel specimen with yield strength lower than 90,000 psi did not show SSC failure above 100°F. As temperature is known to diminish H_2S solubility into brine, it can be understood that the reduction in H_2S concentration causes the reduction in SSC susceptibility, providing safer operation condition at higher temperatures.

2.3.3 Metallurgical Properties

Hardness and alloying elements of the tubulars are of interest in analyzing the SSC resistance. As the SSC resistance decreases with increasing hardness of materials, NACE limits the hardness of carbon steels and low alloy steels to 22 HRC (250 HV) for use in sour condition. Ciaraldi (1986) Performed NACE Method A test on carbon steels with different hardness values and presented the SSC threshold stress as a function of hardness (Fig. 2.4). The threshold stress trend shows that the material

experiences sudden reduction in SSC resistance in the range of 22-24 HRC. Tempering is often applied to reduce the hardness.

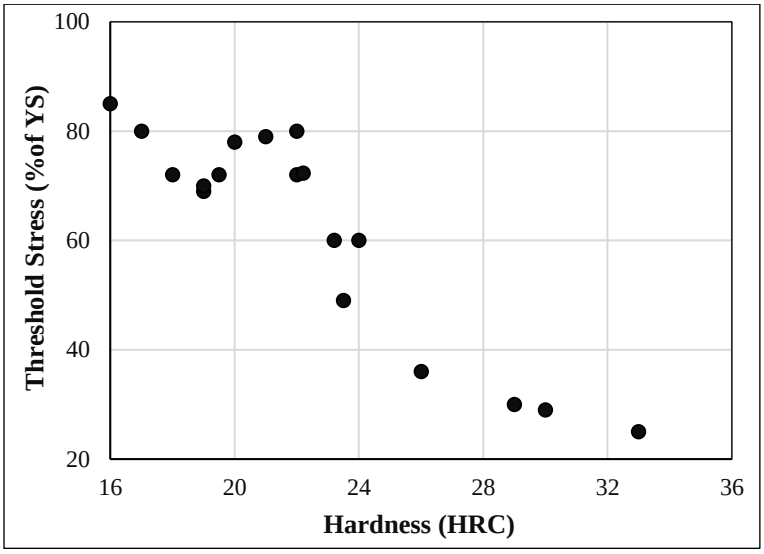


Figure 2.4: Threshold stress vs. Hardness (Tale (2014) redrawing from Ciaraldi (1986))

Another metallurgical properties that affect the SSC susceptibility is alloying elements added to the tubular steel materials with purpose of enhancing the mechanical and thermal properties for better application. Chromium (Cr), Nickel (Ni) and Molybdenum (Mo) are known to have substantial influences on SSC resistance. Increasing amount of Cr reduces the hydrogen permeation rate, by creating thicker protective film on the metal surface. This reduction in hydrogen permeation rate improves the SSC resistance as the film prevents the attack of H_2S. (Kimura et al. 1996) Ni is generally known to have detrimental effect on SSC resistance as it reduces yield strength of the metal when added especially with more than 2%. (Craig et al. 1992) In contrast, Mo improves SSC resistance by reducing the depassivation pH (Hashizume and Inohara 2000). Therefore, in sour environment, Mo embedded carbon steel can perform better than Ni containing steel.

2.4 SSC Measurement

NACE provides four standard laboratory testing methods (NACE TM0177) for SSC resistance (NACE Standard 2009): i) Method A – NACE Standard Tensile Test; ii) Method B – NACE Standard Bent-Beam Test; iii) Method C – NACE Standard C-Ring Test; and iv) Method D – NACE Standard DCB Test.

Method A is developed to investigate the cracking resistance under uniaxial tensile load. A round type test specimen is used under pre-defined stress condition. The SSC susceptibility is evaluated by measuring time to failure. Method B is established to assess cracking failure resistance of steel in SSC environment having wet H_2S at low-pH and stress variation. A compact thin flat shaped specimen is employed for this testing method. In Method C, the cracking resistance of metals are evaluated by exposing a specimen to SSC environment while subjected to a circumferential load (hoop stress). It is often applied to determine the susceptibility of materials to cracking that occur in transverse axis of tubulars or structural bars. In Method D, cracking susceptibility is evaluated in terms of critical stress intensity factor, K_{ISSC} for SSC and K_{IEC} for general cracking. Before the test, a controlled crack is initiated on the specimen to measure the critical stress intensity factor, then a crack-arrest type of fracture mechanics test is conducted.

Among the four methods, NACE Method A is most widely used in SSC testing; however, it requires one month of long test duration, which is problematic when large number of measurement data is required for the investigation. To mitigate the time constraint, Slow Strain Rate Test (SSR Test) or Constant Extension Rate Test (CERT) presented in NACE TM0198 can be combined with Method A to reduce experiment

duration (NACE Standard 2004). SSR Test provides screening method for Corrosion Resistant Alloys (CRAs). It requires relatively short test duration compared to other methods. In this test, the specimen is slowly strained at a constant rate. Therefore, it initiates the cracking in the testing materials. SSR method is generally used to evaluate SSC resistance of stainless steels and nickel-based alloys. In this study, Method A is coupled with SSR Test to reduce test duration. The following sections introduce both methods in detail.

2.4.1 NACE Method A – Tensile Test

In Method A, a cylindrical test specimen with the dimensions described in Fig. 2.5 and Table 2.1 is subject to tensile load, which is equivalent to 80 – 90% of its specified minimum yield strength (SMYS) in sour condition. The testing sour condition for SSC experiment is recommended to have 5% NaCl and 0.5% anhydrous acetic acid solution saturated with H_2S at a temperature of 77°F. Low pH of 2.5-3.5 is claimed to provide more conservative testing result than actual case, since acidic condition increase the SSC susceptibility.

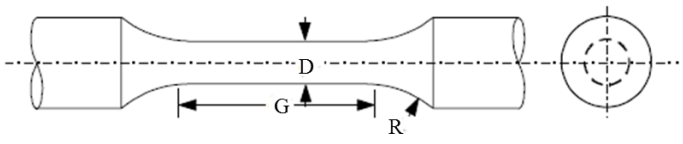


Figure 2.5: Schematic of Method A test specimens (NACE Standard 2009)

Table 2.1: Dimensions of Method A test specimens

Dimensions	Standard tensile test specimen	Subsize tensile test specimen
Diameter (in.)	0.25 ± 0.005	0.15 ± 0.002
Gauge length (in.)	1.00	0.60
Radius of curvature (in.)	0.60	0.60

The test is performed for 720 hours unless the specimen fails. Un-failed samples are etched in solution of nitric acid and alcohol for microscopic examination of cracks. Fractured or cracked materials are not suitable for SSC test because very high tensile load is applied to the specimens. If no cracks appear, the applied stress is deemed below threshold stress of the material, thus the material is considered for use in sour services. Repeated tests under different stress levels are conducted to determine the threshold stress of the tested materials, which is noted as the stress at which the tested specimen survives for 720 hours.

2.4.2 Slow Strain Rate Test

Slow strain rate test is often called Constant Extension Rate Test (CERT). The name refers to the test method which involves slow straining of the specimen to failure at a constant rate. Although this method is developed for SCC resistance testing, the similarity in the mechanism of SSC and SCC enables the method to be used for SSC susceptibility measurement. Researchers have validated the use of CERT for SSC testing with reasonable extent of modification. (Koh et al. 2004, Hörstemeier et al. 2010) In this method, specimens are tested in atmospheric non-corrosive condition and also exposed to sour condition. The stress-strain data were collected to investigate the influence of SSC.

Hörstemeier et al. (2010) performed both NACE Method A and CERT tests on the same templates with SMYS of 110, 125 and 140 ksi to verify the reliability of CERT for SSC susceptibility measurement. In Method A, the time-to-failure data is collected to indicate SSC resistance, while CERT uses the ratio of elongation to failure in atmospheric and sour conditions as computed below:

$$E_pR = \frac{E_{p,sour}}{E_{p,air}} \times 100 \tag{2.3}$$

where E_pR is elongation to failure ratio, $E_{p,sour}$ is plastic elongation to failure in sour condition, and $E_{p,air}$ is plastic elongation to failure in air.

Time-to-failure of Method A and E_pR of CERT method showed a similar trend (Fig. 2.6). The higher is the E_pR, the longer time to failure. Therefore, CERT can replace the Method A SSC resistance criterion.

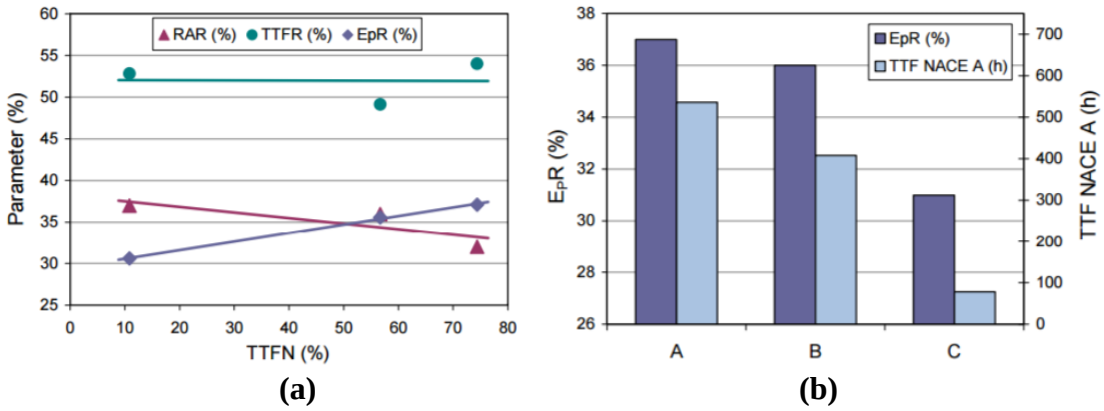


Figure 2.6: Comparison chart between Method A result and CERT E_pR :(a) Dependence of CERT parameter of C-110 materials on normalized time-to-failure of Method A; and (b) Correlation of EpR to average time-to- failure of Method A for C-110 (Hörstemeier et al. 2010)

Koh et al. (2004) also studied the suitability of CERT for SSC testing and found that the mechanical property changes such as ultimate tensile strength, plastic strain to failure and ductility of the specimen resulting from SSC susceptibility can be depicted from a CERT test result. These mechanical properties have been used to evaluate the SSC performance of steels in this study. In the SSC experiment, hollow minipipes were used as testing specimens rather than solid cylindrical rod samples, since hollow shape better represents the actual downhole tubulars and results obtained

from minipipes did not show significant deviation from the result of API full scale SSC test (Cernocky et al. 2005).

2.5 Stress – Strain Prediction from Tensile Test

Downhole tubulars under uniaxial loading undergoes deformational changes and reaches fracture point when the load exceeds a certain limit of material strength. These changes are reflected in mechanical properties of the tubulars and practically noticeable in stress-strain curve. Numerous studies (Ramberg and Osgood 1943; Bridgman 1944; Bridgman 1952; Le Roy et al. 1981; Zhano and Li 1994; Ling 1996; Hibbeler 2011; Dan et al. 2007; Joun et al. 2008; Garbatov et al. 2014; Wang et al. 2016) have simulated the downhole situation using tensile testing setup and generated experimental stress-strain diagrams of different types of metallic materials to analyze and predict their mechanical behavior. The mechanical behavior displayed in those stress-strain diagrams provides the SSC susceptibility of the material. The strength can be used to determine the stress required to initiate plastic deformation or ductility of the materials, which is often related to the SSC resistance (Davis 2004).

In conventional tensile strength test, an engineering stress-strain curve is obtained by presenting the tensile load as a function of elongation. Engineering stress, or nominal stress, σ_e, is defined as:

$$\sigma_e = \frac{P}{A_0} \tag{2.4}$$

where P is the applied load and A_0 is the original cross sectional area of the specimen. The engineering strain, or nominal strain,ε_e, is expressed as:

$$\varepsilon_e = \frac{\Delta L}{L_0} = \frac{L - L_0}{L_0} \tag{2.5}$$

where L_0 and L are the original and final lengths of the specimen. Figure 2.7 demonstrates typical trend of an engineering stress-strain curve for ductile steel, which can be obtained during the tensile test.

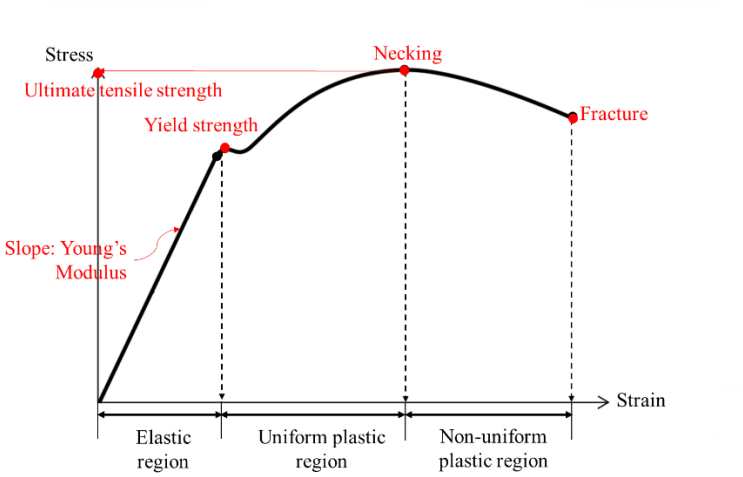


Figure 2.7: Engineering stress-strain curve for ductile steel

As shown in Fig. 2.7, in the elastic deformation region, stress has linear relationship with strain after the adjustment of measuring sensors dead zone at the beginning of the test. Hooke's law can be applied to this region and the slope of stress-strain is known as Young's modulus, or Elastic modulus, representing the level of proportionality. The material returns to its original state after removal of tensile load as far as stress remains in the elastic region. When stress keeps increasing and becomes higher than the yield strength, the material loses its elasticity and enters into plastic region where it will be permanently deformed even after removal of load. Initially, the material stays in the uniformly plastic deformation region. In this region, increase in stress is supported by the material's resistant characteristic to deformation and as a result it experiences strengthening. This is called strain hardening where stress rises continuously but flatter as compared to elastic region. While strain hardening happens,

the cross sectional area of specimen somewhat uniformly diminishes as strain increases. Once it reaches the stress equivalent to ultimate tensile strength, the stress applied for deformation becomes greater than the capacity of the reduced cross sectional area to withstand the stress. Necking happens at this point and further plastic deformation is concentrated in the weakest part of the material resulting in reversal of the trend (Hibbeler 2011; Davis 2004)

Engineering stress-strain curve reasonably explains the mechanical behavior of a material in the elastic region, in which the original material configurations is recovered and applicable material properties can be reasonably predicted. However, it lacks accuracy in the plastic region where strain is comparably large, cross sectional area substantially varies due to necking, and permanent deformation occurs.

True stress-strain curve is introduced to overcome this problem by applying the actual cross sectional area and the instantaneous strain increment to stress-strain calculation. True stress (corrected stress), σ_t, and true strain (corrected stress), ε_t, are expressed using engineering stress (σ_e) and strain (ε_e) as:

$$\sigma_t = \frac{P}{A} = \frac{P}{A_0}\left(\frac{A_0}{A}\right) = \frac{P}{A_0}\left(\frac{L}{L_0}\right) = \frac{P}{A_0}(1+\varepsilon_e) = \sigma_e(1+\varepsilon_e) \tag{2.6}$$

$$\varepsilon_t = \int_{L_0}^{L} d\varepsilon = \int_{L_0}^{L} \frac{dL}{L} = \ln\left(\frac{L}{L_0}\right) = \ln(1+\varepsilon_e) \tag{2.7}$$

These expressions are suitable for elastic region and uniformly plastic region; however, they are not valid for the non-uniform plastic region after necking. Since the material is subjected to localized stress variation with the onset of necking, the cross sectional area for non-uniform plastic deformation should be directly measured rather than being determined from the strain. The following sections present mathematical

models and empirical correlations to describe and predict mechanical behavior of materials from stress-strain curves, which are generally developed for each deformation region.

2.5.1 Elastic Deformation

As previously stated, stress increases proportionally with strain showing linear relationship in elastic region. This relationship is denoted as Hooke's law and mathematically expressed as:

$$\sigma = E\varepsilon \tag{2.8}$$

where E indicates the proportionality constant called Young's modulus or elastic modulus. Both engineering stress and strain obtained from Eqns. (2.4) and (2.5) and true stress and strain calculated by Eqns. (2.6) and (2.7) can be used for the construction of stress-strain curve since those stresses and strains obey Hooke's law in elastic deformation process.

2.5.2 Uniformly Plastic Deformation

The true stress-strain curve in uniformly plastic region is generally expressed by power law. Ludwik (1909) and Hollomon (1945) introduced simple equations to describe stress-strain relationship in the uniformly plastic deformation region:

Hollomon (1945): $\sigma = K\varepsilon^n$ (2.9)

Ludwik (1909): $\sigma = \sigma_0 + K\varepsilon^n$ (2.10)

where σ and ε are true stress and true plastic strain, respectively. K is the strength coefficient, n is the strain hardening exponent, and σ_0 is the yield stress. The strain hardening exponent, n, is given by:

$$n = \frac{d(\ln \sigma)}{d(\ln \varepsilon)} = \frac{\varepsilon}{\sigma}\frac{d\sigma}{d\varepsilon} \tag{2.11}$$

For perfectly elastic materials (solids), $n = 1$. The values of n range from 0.1 to 0.5 for most of metallic materials (Wang et al. 2016).

Similar correlations are developed by other researchers based on the power law type relationship (Dan et al. 2007):

Swift (1952): $\sigma = K(\varepsilon_0 + \varepsilon)^n$ (2.12)

Voce (1948): $\sigma = \sigma_S - (\sigma_S - \sigma_0)\exp(-n\varepsilon)$ (2.13)

Misiolek (1977): $\sigma = K\varepsilon^n \exp(n_1\varepsilon)$ (2.14)

where σ_S is the saturation stress which is the asymptotic stress value obtained after intense deformation and estimated to be close to ultimate tensile strength (Choudhary et al. 2013). Ramberg and Osgood (1943) produced a widely used correlation to interpret the mechanical behaviors in both elastic and uniformly plastic region (Ramberg and Osgood 1943; Garbatov et al. 2014):

$$\varepsilon = \frac{\sigma}{E} + K\left(\frac{\sigma}{E}\right)^m = \frac{\sigma}{E} + \alpha\frac{\sigma_R}{E}\left(\frac{\sigma}{\sigma_R}\right)^m \tag{2.15}$$

where σ_R is the offset yield stress or the proof stress or the reference stress determined at the point corresponding to 0.2% strain (therefore sometimes noted as $\sigma_{0.2}$), and α and m are dimensionless constants defined as $\alpha = K\left(\frac{\sigma_R}{E}\right)^{m-1}$ and $m = \frac{1}{n}$, respectively.

If the true stress, σ, is less than the offset yield stress, σ_R, the material stays in elastic regime and the uniformly plastic deformation term $\alpha \frac{\sigma_R}{E}\left(\frac{\sigma}{\sigma_R}\right)^m$ will be ignored leaving Eqn. (2.15) to become Eqn. (2.16) conforming Hooke's law:

$$\varepsilon = \frac{\sigma}{E} \tag{2.16}$$

However, if the material elongates long enough so that the elastic strain is negligible compared to the uniformly plastic strain, $\frac{\sigma}{E}$ is assumed to be negligible, and Eqn. (2.15) yields:

$$\varepsilon = \alpha \frac{\sigma_R}{E}\left(\frac{\sigma}{\sigma_R}\right)^m \tag{2.17}$$

This correlation can be expressed in terms of stress as:

$$\sigma = \left(\sigma_R\left(\alpha \frac{\sigma_R}{E}\right)^{1/m}\right)\varepsilon^{1/m} = \left(\sigma_R\left(\alpha \frac{\sigma_R}{E}\right)^{n}\right)\varepsilon^{n} = K'\varepsilon^{n} \tag{2.18}$$

Equation (2.18) again indicates the power law characteristics presented in other correlations, Eqns. (2.9), (2.10), and (2.12 – 2.14).

2.5.3 Non-uniform Plastic Deformation after Necking

Once necking happens, the assumption applied in the uniformly plastic deformation cannot be applied. In fact, the decrease in cross sectional area is not proportional to the elongation. Structural instability induced from non-uniformities interrupts the uniform uniaxial stress being applied. Therefore a multiaxial stress state arises in the necking region and makes it impossible to extrapolate the uniformly plastic deformation correlations.

Analytical Method

Bridgman (1944, 1952) developed an analytical correction method to analyze the stress-strain curve of uniaxial cylindrical tensile specimen with several assumptions in stress distribution and the geometry of necking region. Due to the instantaneous non-uniform deformation in the necking region, the equivalent stress-strain relationship at the minimum cross sectional area is of interest to describe the true stress-strain curve. In this model, the first assumption is that strain is uniformly distributed in the minimum cross section as denoted below:

$$\varepsilon_r = \varepsilon_h = -\frac{\varepsilon_t}{2} \tag{2.19}$$

where ε_r is the radial strain, ε_h is the hoop strain, and ε_t is the true axial strain, which is expressed as $\varepsilon_t = \ln(1+\varepsilon_e)$. The second modeling assumption is that the ratios of the axial stress while tensile loading remain constant, the equivalent strain at the minimum section, $\bar{\varepsilon}$, can be considered as the true axial strain or the average axial strain. Applying the volume conservation concept, the equivalent strain is expressed as:

$$\bar{\varepsilon} = \varepsilon_t = \ln\frac{A_0}{A} = 2\ln\frac{D_0}{D} \tag{2.20}$$

where D is the diameter of the smallest cross section. Unlike the equivalent strain, the equivalent stress, $\bar{\sigma}$, is not equal to the true axial stress or average axial stress, since the radial and hoop stresses are not zero after necking. Average axial stress, $\sigma_t = \sigma_e(1+\varepsilon_e)$. The radial, hoop and true axial stresses are calculated with the assumption that the specimen experiences deformation in the necking region as described in Fig. 2.8, and curvature of the subjected longitudinal grid line is defined as:

$$\frac{1}{\rho} = \frac{r}{aR} \tag{2.21}$$

where ρ is the radius of curvature of the subjected grid line, r is the radius of actual cross section, a is the radius of the minimum cross section and $a = \frac{D}{2}$, and R is the radius of curvature of the neck.

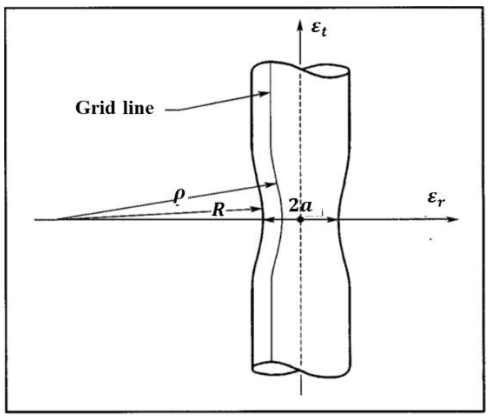


Figure 2.8: Necking geometry used in Bridgman correction method (Ling 1996)

Bridgman (1952) suggested the following distribution of the three stresses at the minimum cross section:

$$\sigma_r = \sigma_h = \frac{(\sigma_t)_{av}}{\left(1+\frac{2R}{a}\right)}\left[\frac{\ln\left(\frac{a^2+2aR-r^2}{2aR}\right)}{\ln\left(1+\frac{a}{2}R\right)}\right] \text{ and}$$

$$\sigma_t = \frac{(\sigma_t)_{av}}{\left(1+\frac{2R}{a}\right)}\left[\frac{1+\ln\left(\frac{a^2+2aR-r^2}{2aR}\right)}{\ln\left(1+\frac{a}{2R}\right)}\right] \tag{2.22}$$

By applying the assumption of von-Mises yield criterion, the equivalent stress at the center of the minimum cross section can be calculated as below:

$$\bar{\sigma} = \sqrt{\frac{1}{2}\left[(\sigma_t - \sigma_r)^2 + (\sigma_r - \sigma_h)^2 + (\sigma_h - \sigma_t)^2\right]} = \frac{(\sigma_t)_{av}}{\left(1 + \frac{2R}{a}\right)\ln\left(1 + \frac{a}{2R}\right)} = k(\sigma_t)_{av} \tag{2.23}$$

where k is regarded as correction factor to transform the average axial stress in the necking region into the equivalent stress to be used in stress-strain analysis. (Bridgman 1952; Ling 1996; Wang et al. 2016)

Even though Bridgman's correction method predicts the mechanical behavior beyond necking fairly well, it accompanies some limitations in practical situations. The biggest problem is that it requires numerous iterations of test with different loads to obtain the radius of actual cross section (r) and the radius of curvature of the neck (R) to be used in the stress calculation, which barely guarantees the sufficient accuracy in the measurement.

Bridgman (1944) provided a simple approximation to determine the ratio of r to R in the large axial strain regime:

$$\frac{a}{R} = \sqrt{\varepsilon_t - 0.1}, \text{ when } \varepsilon_t > 0.1 \tag{2.24}$$

Le Roy et al. (1981) also derived an empirical correlation for the ratio between r and R; however, its application is restricted to a certain range of pressure and dependent on the void size of the material, which is defined as:

$$\frac{a}{2R} = 0.555(\varepsilon_r - \varepsilon_u) \tag{2.25}$$

Numerical Method

Recent approaches that determine the true stress-strain curve in non-uniform plastic deformation region extensively deploy Finite Element Method (FEM). FEM

targets the actual experimental stress-strain results and searches for a best-fit stress-strain model by modifying material parameters used in the equations of FEM simulation through iterative computations. Once the error between the experimental stress and simulated stress becomes less than a predefined limit, the final simulated parameters are determined to construct the true stress-strain curve. Most of the numerical stress-strain models in FEM simulation are based on the power law constitutive relation. Misiolek model (Eqn. 2.14) has been successfully used as an embedded correlation in a software with different parameters found in the trial-and-error process (Zhano and Li 1994; Joun et al. 2008; Wang et al. 2016).

Ling (1996) combined power law functions with linear functions and introduced the weighted average method to compensate for the conservative limitations of power law application. The proposed equation has the lower and upper limits of true stresses. The weight parameter in the equation is adjusted by iterative calculations using FEM software. The upper and lower limits are introduced to prevent excessive extrapolation resulting from power law model, which is adopted from the uniformly plastic deformation analysis. The model developed by Ling (1996) is presented as:

$$\sigma = \sigma_u \left[w(1+\varepsilon+\varepsilon_u) + (1-w)\left(\frac{\varepsilon^{\varepsilon_u}}{\varepsilon_u{}^{\varepsilon_u}} \right) \right] \tag{2.26}$$

where w is an unknown weight parameter with $0 \le w \le 1$.

CHAPTER 3: EXPERIMENTAL STUDY

This chapter introduces the laboratory test setups and procedures to investigate the embrittlement behavior of tubulars by simulating the downhole SSC condition. Tensile Strength Testing (TST) apparatus and Sulfide Stress Cracking (SSC) cell are developed to carry out the experiment using three different grades of API carbon steels (T-95, C-110 and Q-125).

3.1 Measuring Strategy

TST apparatus is a mechanical device to obtain stress-strain profile of a test specimen (minipipe) after exposure to corrosive environment (i.e. brine saturated with mixed gas containing methane, CO_2 and small amount of H_2S). The SSC cell simulates the downhole environment. During this investigation, cell temperature was maintained at 100°F, and outside and inside pressures of the minipipe were held at 4,000 psi and 6,000 psi, respectively while the specimen was subjected to a constant tensile stress load of 85% of its yield stress. Test measurements were conducted in the following sequence of stages:

Stage 1. Baseline Measurement

A clean minipipe was strained to failure in TST apparatus without SSC aging to evaluate the changes in stress-strain data of the test specimens before exposure to the corrosive environment. Baseline measurements are used to establish the baselines which provide reference mechanical properties of each steel grade which are compared with those of the exposed specimens.

Stage 2. Elasticity check before SSC test (Limit Test)

Upon baseline properties were obtained from Stage 1, each specimen was strained to 80% of its elastic limit in TST apparatus before it was exposed to the corrosive environment in SSC cell. Each measurement was repeated three times to ensure the specimen elasticity and check inherent crack or defect.

Stage 3. Exposure to SSC Condition (Corrosion Test)

After testing in Stage 2, the specimen was cleaned to remove stains on the gauge section and installed in SSC cell. Then, for seven days, the specimen was exposed to the corrosive environment in SSC cell. Pressure in the SSC cell was pre-determined to achieve the desired H_2S and CO_2 partial pressures. A tensile stress load of 85% of yield stress of the specimen was applied during the exposure.

Stage 4. Limit Test Followed by Failure Test

The specimen was recovered from SSC cell after one week and examined again with TST apparatus to acquire new stress – strain data. The specimen was stretched to 80% of its elastic limit two times, then stretches to failure at the third trial. The stress-strain curve from the final trial provides mechanical properties after exposure to SSC condition, which includes yield strength, ultimate tensile strength, and plastic strain to failure. Changes in the mechanical properties from baseline obtained in Stage 1 are expected to indicate the degree of brittleness of the test specimen.

3.2 Test Materials

The test specimen is a round hollow carbon steel minipipe with grade of T-95, C-110 and Q-125. The three grades of specimens are cut from API casing pipe stocks.

API provides specification for steel tubular products for use in oil and gas fields. T-95 and C-110 are designed for deep sour condensate wells. Q-125 targets high-pressure deep wells; however, it is generally not recommended like T-95 and C-110 for sour condition because it is sensitive to SSC due to its high yield strength. (Morana and Nice 2009) The chemical compositions of each steel grade used in this study are presented in Table 3.1 as weight percentage (%).

Table 3.1: Chemical compositions of tested carbon steels

Steel grade	Elements (Wt %)									
	C	**Mn**	**P**	**S**	**Si**	**Cu**	**Ni**	**Cr**	**Mo**	**Fe**
T-95	0.33	0.34	0.009	<0.001	0.27	0.02	0.03	1.01	0.79	Remainder
C-110	0.30	0.47	0.007	0.001	0.23	0.01	0.01	1.01	0.78	Remainder
Q-125	0.26	0.49	0.012	<0.001	0.21	0.03	0.04	0.91	0.26	Remainder

The dimensions of specimen are presented in Table 3.2 and Fig. 3.1. During the tests, both ends of the specimen were screwed to metal adapters and installed on the TST apparatus or SSC cell.

Table 3.2: Dimensions of test specimen*

Distance	Dimension (in)	Distance	Dimension (in)
Overall length	4.00	Gauge section outer diameter	0.375
Distance between threads	3.00		
Distance between shoulders	2.00	Gauge section inner diameter	0.312
Gage length	1.75		

*For the dimensions specified in Table 3.2, the tolerance limits are 0.005 inches.

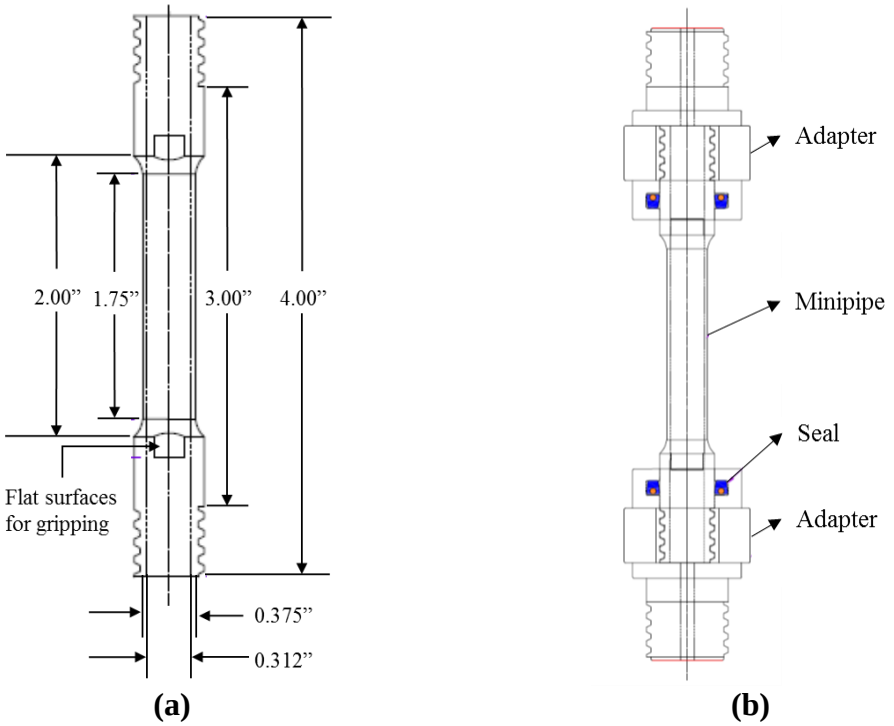


Figure 3.1: Test specimen: a) without adapters; and b) with adapters

3.3 Test Apparatuses Used During the Investigation

3.3.1 TST Apparatus

A schematic of TST apparatus is presented in Fig. 3.2. The apparatus has three main components:

i. Structural frame of hydraulic cylinder and flange plate

A double acting hydraulic cylinder is used for stretching the specimens. Two holders are used to connect the specimen to the hydraulic piston rod and the structural frame. The top specimen adapter is attached to a flange plate, which is bolted to the structural frame. The bottom adapter is mounted on piston rod of the hydraulic cylinder using a coupler. During the test, the upper part of the specimen remains stationary while the lower part is pulled down by the hydraulic cylinder.

ii. Pressurization system

High-pressure oil is used to pressurize the hydraulic cylinder. The oil is pumped into the cylinder using a flow rate-controlled syringe pump. The piston is forced by the oil to apply tensile load to strain the specimen. Speed controller is used to maintain the stress loading rate of approximately 55,000 psi/min in accordance with ASTM standard.

iii. Instrumentation and data acquisition system

Loading stress is determined from hydraulic pressure reading of a pressure transmitter. Strain is determined from reading of an elevation sensor which is attached to the hydraulic piston coupler. Using the elevation sensor change in specimen length is measured and converted to strain and recorded by the data acquisition system (computer with data acquisition card). The hydraulic pressure is also monitored and recorded using the data acquisition system.

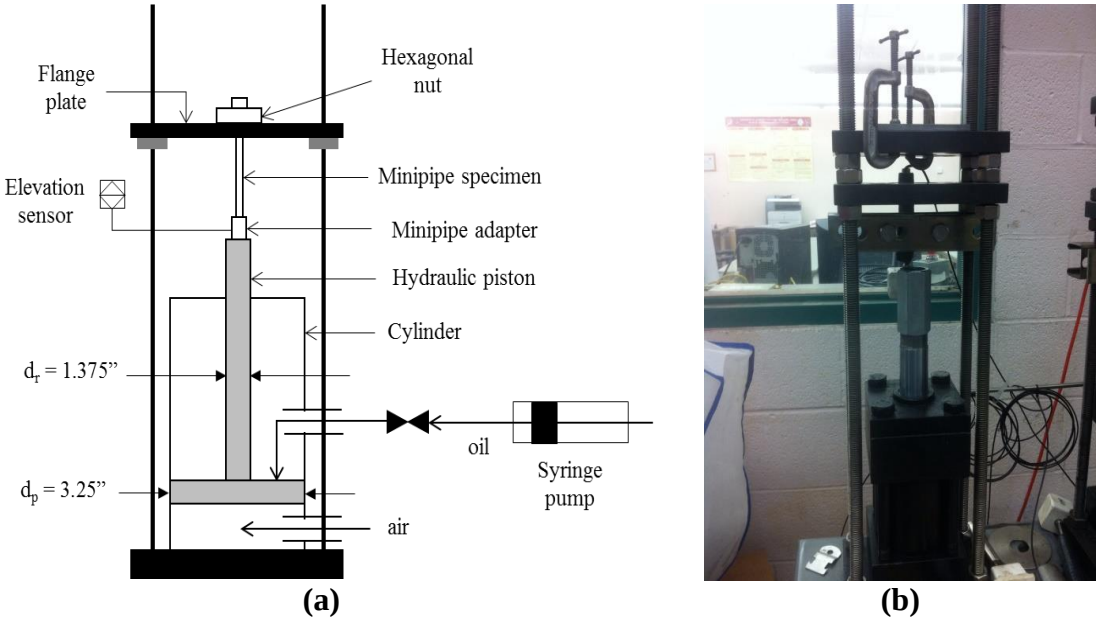


Figure 3.2: TST apparatus: a) schematic; and b) picture

3.3.2 SSC Test Schematic

Figure 3.3 displays an overall schematic of the SSC test setup, which includes: i) SSC aging cell; ii) gas storage cylinders; iii) gas injection cylinder; iv) pneumatic cylinder with N_2 gas; v) gas and heating fluid lines; and vi) instrumentation / valves and data acquisition system.

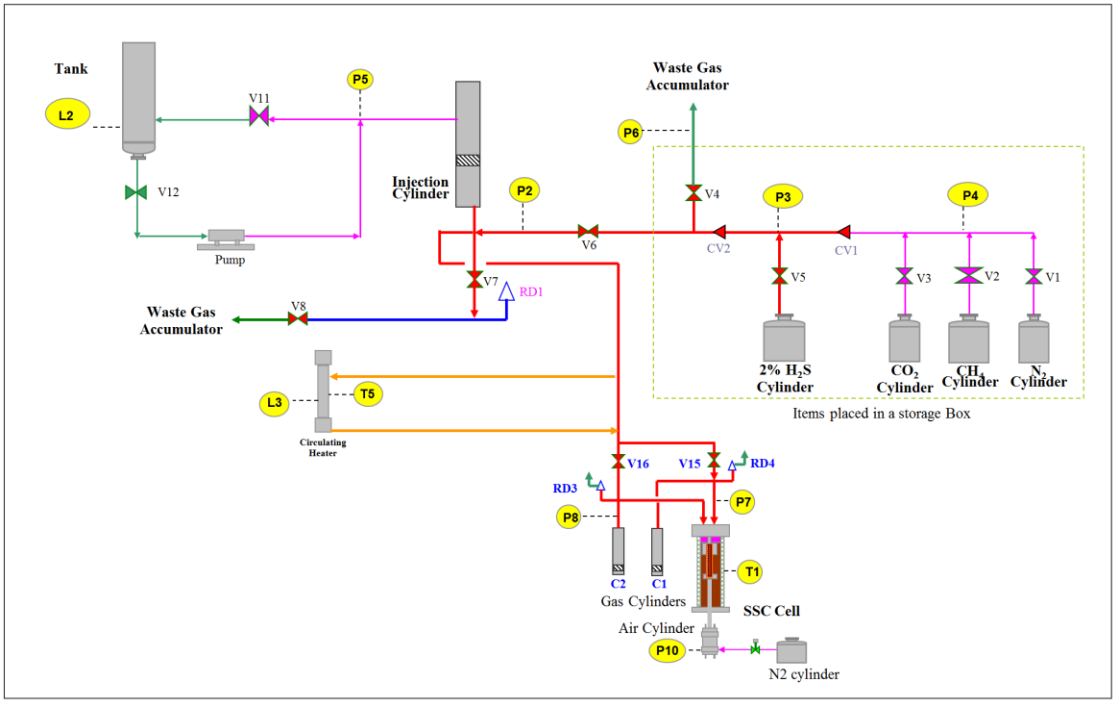


Figure 3.3: SSC test schematic

H_2S, CO_2 and CH_4 were the main test gases. H_2S gas was supplied as a mixed gas mostly containing CH_4 specific H_2S concentrations (300 ppm and 500 ppm). The 300 ppm H_2S mixed gas was used for lower CO_2 concentration tests (0% and 2.5%) and the 500 ppm H_2S was utilized for higher CO_2 concentration (more than 2.5%) tests. Pure CH_4 and CO_2 gas supply were also used to create the test environment.

When a test specimen was installed inside SSC aging cell, test gases were first pressurized in the injection cylinder before flowing into the cell because the gases were supplied at pressures lower than 2,500 psi. Injection cylinder also served as a gas metering device to control gas composition in the cell.

After pressured, the gases were injected into the cell by opening the valves, V15 and V16. The injection gases fill not only the cell but the gas cylinders directly connected to the cell. Each gas cylinder is connected to inside or outside of a minipipe specimen installed in the SCC cell. Since the cell and minipipe do not hold sufficient amount of gas during the test, the cylinders are necessary to provide additional gas volume to maintain the cell pressure. The minipipe sits inside the cell and the surrounding space is filled with 2% NaCl brine solution. V15 is connected to the inside hollow of a minipipe and V16 is connected to the outside of the minipipe. During the test, V15 and V16 were controlled to increase the cell pressure gradually up to 4,000 psi inside and outside of minipipe. When the outer and inner pressure reached 4,000 psi, V16 was closed while V15 remained open to inject more gases into the inner part of the minpipe to increase the pressure to 6,000 psi. Pressure transducers (P7 and P8) are installed to measure specimen inside and outside pressures. A temperature sensor (T1) is connected to the inside of the cell to measure cell temperature during the test. Test pressures and temperature are monitored and recorded during the experiment.

After injecting the gases and pressurizing the minipipe inside and outside, tensile load is applied using a pneumatic (air) cylinder, which is actuated by nitrogen gas supply pressure (P10) as shown in Fig. 3.3. The cylinder is attached to the bottom of SSC cell and directly connected to a pulling rod. During the test, the upper end of

the specimen is tied to the cell lid and the lower end is fastened to the pulling rod. Therefore, the specimen experiences vertical load when the rod is pulled downward by the pneumatic cylinder (Fig. 3.4a). Pneumatic pressures required to produce stress level of 85% of the nominal yield strength of the specimens are computed in Section 3.3.3.

3.3.3 SSC Cell

The SSC cell is where the corrosion process takes place on the surface of specimen (Fig. 3.4b). The cell a pressure vessel with top and bottom lids. The pulling rod, which passes through the bottom lead is connected to the specimen holder. During the test, a specimen was connected to the top lid and the pulling rod using adaptors. Two o-ring seals are applied in the cell for the purpose of complete isolation of specimen inside and outside pressures. The SSC cell top lid holds two opening holes which allow gas injection into inner and outer parts of the specimen. Mixed gas is injected through these holes to pressurize both sides (inside and outside) of the specimen. The pulling rod connected to the pneumatic cylinder pulls the specimen to simulate tensile loading condition occurring downhole. The required pneumatic pressure is calculated based on tensile loading of the specimen resulting stress level of 85% of nominal yield strength of the steel grade. Thus, the tensile stress in the specimen, S_{ts}, is expressed as:

$$S_{ts} = \frac{F}{A} = \frac{F}{\frac{\pi}{4} \times (d_o^{\,2} - d_i^{\,2})}$$

where F is total hydraulic pressure force acting on the specimen, d_o and d_i are outer and inner diameter of the gauge section of the specimen, respectively. $d_o = 0.375\ in.$

and $d_i = 0.312\ in.$ Considering hydraulic force acting inside and outside of the specimen during the test, the tensile stress in the specimen can be expressed as:

$$S_{ts} = \frac{P_{in} \times \frac{\pi}{4} \times d_i^{\,2} + P_{out} \times \frac{\pi}{4} \times (d_{sr}^{\,2} - d_o^{\,2}) + P_{pneu} \times \frac{\pi}{4} \times (d_c^{\,2} - d_{sr}^{\,2})}{\frac{\pi}{4} \times (d_o^{\,2} - d_i^{\,2})} \tag{3.1a}$$

where d_c is diameter of SSC cell cylinder plate, and d_{sr} is diameter of SSC cell pulling rod. $d_c = 4.5\ in.$ and $d_{sr} = 0.875\ in.$

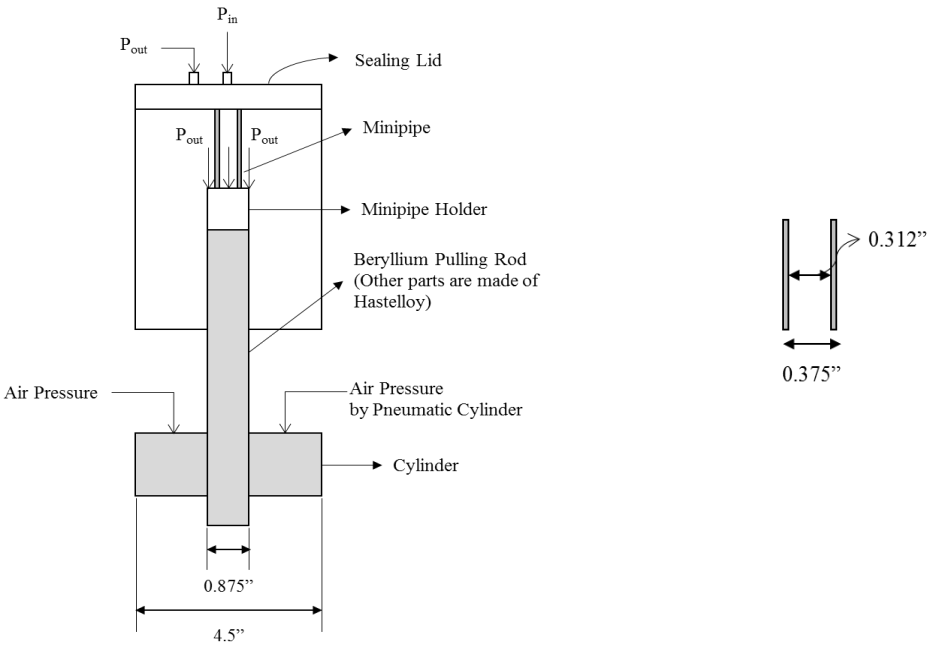
During the corrosion test, the stress level should be 85% of nominal yield strength, f_y. Thus:

$$S_{ts} = 0.85 \times f_y \tag{3.1b}$$

Combining Eqns. (3.1a) and (3.1b), the pneumatic pressure is computed as:

$$P_{pneu} = \frac{(0.85 \times f_y) \times \frac{\pi}{4} \times (d_o^{\,2} - d_i^{\,2}) - P_{in} \times \frac{\pi}{4} \times d_i^{\,2} - P_{out} \times \frac{\pi}{4} \times (d_{sr}^{\,2} - d_o^{\,2})}{\frac{\pi}{4} \times (d_c^{\,2} - d_{sr}^{\,2})} \tag{3.2}$$

where $P_{in} = 6{,}000\ psi$ and $P_{in} = 4{,}000\ psi$



(a) **(b)**

Figure 3.4: SSC Cell: a) Schematic; and b) Side view of specimen gauge section

3.4 Test Conditions

When specimens are tested in TST apparatus to obtain stress-strain data, the hydraulic pressure in the TST apparatus is computed based on the expected stress level in the specimen. The hydraulic force acting on the piston (Fig. 3.2) can be expressed as:

$$F = P \times \frac{\pi}{4} \times (d_p^2 - d_r^2) \tag{3.3}$$

where P is oil pressure applied to the TST apparatus to push hydraulic piston, d_p is diameter of piston plate, and d_r is diameter of piston rod.

The force can be also expressed using the stress level in the minipipes as; $Force\ (F) = Stress(S) \times Area(A)$. Using dimensions in Figs. 3.2 and 3.4, the stress in the sample is given as:

$$S = \frac{F}{A} = \frac{P \times \frac{\pi}{4} \times (d_p^2 - d_r^2)}{\frac{\pi}{4} \times (d_o{}^2 - d_i{}^2)} \tag{3.4}$$

By substituting the value of 80% of the yield stress for the stress in Eqn. (3.4), the maximum pressure required to perform a limit test (i.e. strength test in which samples are stretched up to 80% of their nominal yield stress level) can be determined for each steel grade (Table 3.3). Similarly, the maximum hydraulic pressure required to perform a complete strength test (failure test) can be calculated.

Table 3.3: Hydraulic pressure required for TST test

Grade	Baseline			Before exposure		After exposure	
	Cal, psi	Set, psi	Failure, psi	Cal, psi	Set, psi	Cal, psi	Set, psi
T-95	380	380	530	424	380	380	380
C-110	440	420	555	444	420	440	440
Q-125	500	500	760	608	550	500	500

Cal = calculated pressure to apply 80% of the yield stress, Set = actual setting pressure for tests, and Failure = measured failure pressure of baseline specimen

For the first and second baseline specimen limit tests, the elastic limits are deemed nominal yield strength of the materials. Hence, 80% of 95,000 psi, 110,000 psi and 125,000 psi are put in the Eqn. (3.4) for T-95, C-110 and Q-125, respectively. For limit tests conducted on unexposed specimen, measured yield strength obtained from the baseline failure test was used. However, the measured strength was not used in the limit tests of exposed specimens. This is to prevent premature failure during the limit test as a result of embrittlement phenomena occurring during SSC test.

The maximum limit test pressure value for C-110 baseline specimen involves a safety margin of 20 psi while those of T-95 and Q-125 do not. The reason for this is, for T-95 and Q-125 grades, that the baseline tests were repeated; therefore, the measured failure pressures were more reliable than the one used for C-110, which was obtained from a single baseline specimen test. As a result, each C-110 specimen had a safety margin of 20 psi when it undergoes the limit test before exposure.

During the SSC test, the specimens were placed in brine (2% NaCl solution) saturated with mixed gas containing different concentrations of CO_2 (0% to 40%). Table 3.4 shows the testing conditions for all specimens used in the experiment.

Table 3.4: Testing conditions for SSC experiment

Grade	Test no.	Temp ˚F	Total Pressure, psi			Gas Composition			Duration, days
			Inside	Outside	Pneu-matic*	H_2S, ppm	CH_4, %	CO_2, %	
T-95	1	0	0	0	21	0	0	0	0
	2	100	6000	4000	21	0	100	0	7
	3	100	6000	4000	21	300	100	0	7
	4	100	6000	4000	21	293	97.5	2.5	7
	5	100	6000	4000	21	300	95	5	7
	6	100	6000	4000	21	300	90	10	7
	7	100	6000	4000	21	300	85	15	7
	8	100	6000	4000	21	300	75	25	7
	9	100	6000	4000	21	300	75	25	7
	10	100	6000	4000	21	300	60	40	7
C-110	1	100	6000	4000	50	0	100	0	15
	2	0	0	0	50	0	0	0	0
	3	100	6000	4000	50	300	100	0	7
	4	100	6000	4000	50	293	97.5	2.5	7
	5	100	6000	4000	50	285	95	5	7
	6	100	6000	4000	50	270	90	10	7
	7	100	6000	4000	50	270	90	10	7
	8	100	6000	4000	50	270	90	10	7
	9	100	6000	4000	50	255	85	15	7
	10	100	6000	4000	50	255	85	15	7
	11	100	6000	4000	50	300	75	25	7
	12	100	6000	4000	50	300	75	25	7
	13	100	6000	4000	50	300	60	40	7
	14	100	6000	4000	50	300	60	40	7
Q-125	1	0	0	0	78	0	0	0	0
	2	100	6000	4000	78	0	100	0	7
	3	100	6000	4000	78	300	100	0	7
	4	100	6000	4000	78	293	97.5	2.5	7
	5	100	6000	4000	78	300	95	5	7
	6	100	6000	4000	78	255	90	10	7
	7	100	6000	4000	78	300	85	15	7
	8	100	6000	4000	78	300	75	25	7
	9	100	6000	4000	78	300	75	25	7
	10	100	6000	4000	78	300	60	40	7

Measurements of Test No. 1 through 11 of C-110 are obtained from Tale (2014).
*Pneumatic pressures for T-95 = 21 psi, C-110 = 50 psi, and Q-125 = 78 psi are calculated considering 85% stress level during corrosion test.

The experimental investigation was initiated with C-110 carbon steel and continued with other steel grades (T-95 and Q-125). The first specimen of C-110 (Test No. 1) was set to SSC cell and exposed to brine saturated with pure CH_4 gas to validate the pressure holding capability of the cell. Test No. 2 for C-110 and Test No. 1 for T-95 and Q-125 were baseline specimen tests.

3.5 Test Procedure

The overall TST – SSC test for each steel grade minipipe specimen was demonstrated per the four stages discussed in Section 3.1. The procedures are explained in detail in the following statements:

Stage 1. Baseline measurement

In this stage, a clean unexposed specimen is prepared and tested to obtain baseline mechanical properties including ultimate tensile strength, plastic strain to failure as well as the crack features, which are used to evaluate exposed specimen. This measurement is conducted only one time for each steel grade, following the procedure outlined below:

i. The uncorroded specimen was attached to the top and bottom minipipe holders then connected to the flange (which is connected to the top holder) and the hydraulic piston (Fig. 3.2).

ii. Pressure corresponding to 80% of nominal yield strength plus a safety margin was set as the maximum limit for hydraulic pressure in the data acquisition system.

iii. Oil was pumped using a syringe pump to the hydraulic cylinder to increase the pressure at a controlled rate to the maximum set pressure

value. The pressure and elevation data collected during the test was automatically converted to stress-strain values for monitoring and control. This way over stretching of the specimen was avoided.

iv. Once the tensile stress in the specimen reaches 80% of elastic limit (yield stress), the oil flow was stopped and the piston was moved backwards to the initial elevation level using compressed air and reversing the syringe pump. When the specimen returned to its initial position, the air supply hose is released.

v. Steps from i to iv were repeated two times to check if the specimen is eligible for the experiment without any crack before strained beyond elastic region. In the third trial, the maximum pressure was set to 1,000 psi in the data acquisition system to break the specimen by gradually exerting tensile load, which was higher than the ultimate strength.

vi. Stress-strain data until the fracture point were obtained. The ultimate tensile strength, plastic strain to failure, and actual yield strength are determined from the stress-strain data. The hydraulic piston moves backwards to the initial elevation level, then the minipipe is disconnected from TST apparatus.

Stage 2. Stress-Strain measurement before SSC test

Same procedures in baseline measurement were performed for the specimens to be used in SSC test with different setting pressure values.

i. Step i to iv of Stage 1 were repeated three times without breaking the specimen (i.e. just stretching it to 80% of its yield value).

ii. Once the minipipe specimen was confirmed of having no inherent crack, it was disconnected from TST apparatus for SSC test.

Stage 3. Exposure to SSC Condition (Corrosion Test)

After straining in TST apparatus, the gauge section of the specimen is cleaned using stain remover (methyl-ethyl ketone) before installed in SSC cell. The specimen was tested in the SCC cell for seven (7) days. The following procedure was applied during the test:

i. The minipipe specimen was attached to the bottom holder of the SSC cell by thread connection as shown in Fig. 3.4. It was then lowered into the cell and inside and outside of the specimen were filled with 2% NaCl brine solution.

ii. The cell was assembled with lid and completely sealed with bolt connection. Inner and outer gas injection lines, and thermometer line were connected to the cell and tightened to prevent any gas leak.

iii. The cell was purged with nitrogen gas for 30 mins at 2,000 psi to deaerate the solution and check leakage and pressure communication between inside and outside of the specimen.

iv. Once the cell and the specimen were ready for the experiment, the temperature was adjusted to the desired level and test gases were injected in to the cell at pre-determined pressures. The pressurization of inside and outside of the specimen takes place simultaneously until the total pressure reaches 4,000 psi, respectively. As this is the pre-determined outer pressure, more gases are injected to the inside of the specimen to fulfill

the inner pressure requirement of 6,000 psi. Pressure equalization between the inner and outer parts indicates the failure of specimen in the cell while it is under tensile load in SSC condition.

v. The specimen was kept in SSC cell until seven days or failure occurs. The maximum test duration is selected because studies (Kermani and MacCuish 1990) showed that the materials are susceptible to SSC related failure within 100 – 200 hours of exposure to the corrosive sour environment. During the corrosion test, test pressures and temperatures (Fig. 3.3) were monitored and automatically recorded by the data acquisition system. The inner and outer pressures of the specimen were decreasing slightly during the test due to dissolution and consumption. As a result, slightly higher gas pressure was maintained in the injection lines during the initial pressurization.

vi. SSC cell was depressurized and cooled down after seven (7) days unless the specimen fails during the test. The gases were sent to the vent line at a sequential order. After opening the cell lid, samples of brine solution were taken from inside and outside of the specimen and stored for further research.

vii. The corroded specimen was recovered from SSC cell and prepared for failure test (Stage 4 in TST apparatus).

Stage 4. Failure test

A specimen that did not fail in the SSC cell, was strained in TST apparatus to obtain mechanical properties after exposure. This stage follows the same

procedure as the baseline measurement: two straining trials up to 80% of elastic limit, and the final straining to failure.

i. The specimen collected from SSC cell was placed in TST apparatus and step i to iv of Stage 1 were repeated two times without breaking the specimen.

ii. The maximum hydraulic pressure of TST apparatus was set at 1,000 psi for the third trial to reach specimen failure point and to acquire a complete stress-strain data to determine mechanical properties. The ultimate tensile strength, plastic strain to failure, and actual yield strength for the specimen after H_2S exposure are calculated from the stress-strain measurements.

iii. For a specimen that fails during SSC test, step i and ii were not performed. The plastic strain to failure is considered to be 0. The ultimate tensile strength is estimated as the total stress calculate using P_{in}, P_{out} and P_{pneu} values which were recorded right before the failure. The actual yield strength cannot be obtained from SSC test.

iv. Changes occurring in mechanical properties of specimen after SSC test compared to the values of baseline specimen indicates the level of embrittlement due to sour corrosion.

Stage 5. Fracture analysis

In this stage, fracture analysis was conducted. The specimen was examined using a digital microscope to determine the type of failure in terms of crack features. The specimen fragments were then stored in a sealed plastic vial with proper labelling.

CHAPTER 4: DATA ANALYSIS AND INTERPRETATION

Using the test setups and procedures described in Chapter 3, SSC susceptibility of API carbon steels has been investigated experimentally. During the test, specimens were exposed to high-pressure sour corrosive environment while subjected to a constant tensile load. Three types of carbon steel grade specimens (T-95, C-110, and Q-125) were used during the test as presented in Table 3.1;

4.1 Mechanical Properties

As discussed in Chapter 2, the engineering stress and strain measurements are converted into true stress and strain values. Each of engineering stress-strain curve is divided into three regions: elastic deformation, uniform plastic deformation to necking and non-uniform plastic deformation after necking. The analysis in this study is based on the true stress and strain profiles using Hooke's law for analytical simplicity. The analysis mainly focuses on the variation in stress curve and strain length in elastic and uniform plastic deformation regions to determine ductility and brittleness of the specimen after SSC experiments.

Tables from 4.1 to 4.3 summarize mechanical properties obtained from the true stress-strain curves of exposed (corroded) specimens. To determine yield strength from the stress-strain diagram, 0.2% offset method is applied. A parallel line to the Young's modulus line (slope of stress-strain in elastic region) is drawn at a strain level of 0.2% along the strain-axis (horizontal axis). The y-coordinate of a certain point where this parallel line intersects the stress – strain curve is called the 0.2% offset yield strength. Plastic strain to failure is read based on the strain corresponding to the 0.2% offset yield

strength. Figure 4.1 shows sample estimation of 0.2% offset yield strength for T-95 baseline specimen.

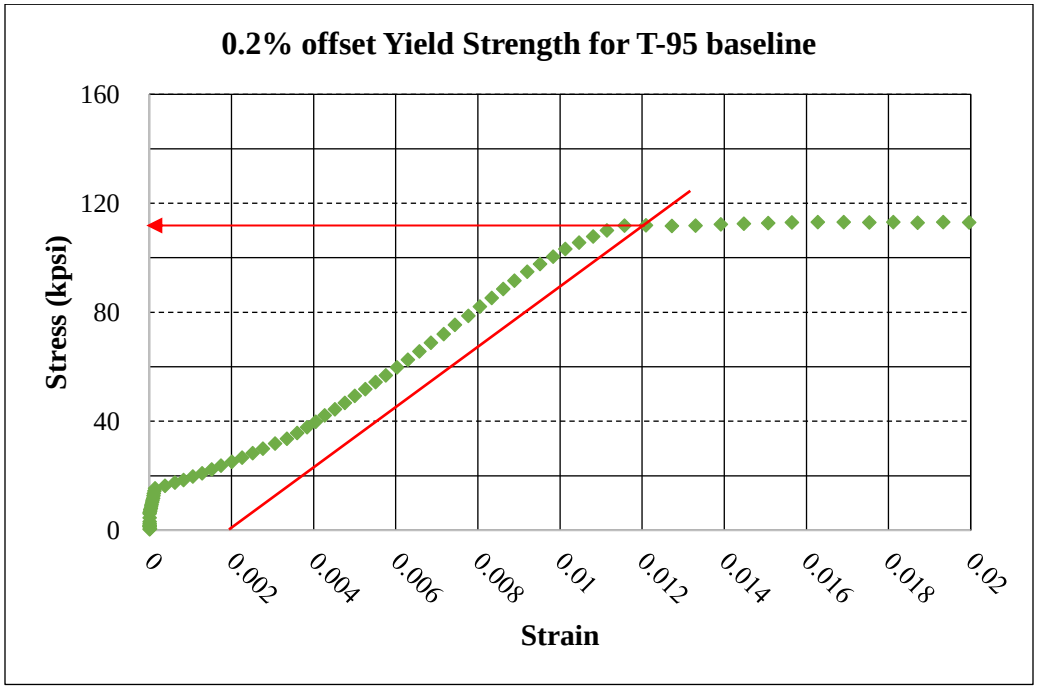


Figure 4.1: 0.2% offset yield strength measurement for T-95 baseline specimen

Among the measured mechanical properties, ultimate tensile strength (UTS) and plastic strain to failure (PSF) are selected to quantify the brittleness of both unexposed and exposed specimens. Yield Strength (YS) measurements are not used in the analysis because they do not show consistent trend due to thickness change in gauge section of the specimen while corrosion test is performed.

Specimens T-95-1 and Q-125-1 and C-110-2 are baselines, which were strained to failure without exposure to any sour environment. They provide the benchmark properties including actual strength to evaluate level of embrittlement through change in mechanical properties. Specimen C-110-1 is the first minipipe tested in SSC cell to confirm the pressure holding capacities of the cell and minipipe for succeeding

experiments. The specimen is aged under pure CH_4 without H_2S and CO_2 gases as shown in Table 4.2.

Table 4.1: Mechanical properties of T-95 specimens after SSC test

No.	H_2S (ppm)	CO_2 (%)	CH_4 (%)	Before Exposure			After Exposure		
				YS, kpsi	UTS, kpsi	PSF	YS, kpsi	UTS, kpsi	PSF
T-95-1	-	-	-	110	139	0.121	-	-	-
T-95-2	0	0	100	-	-	-	110	134	0.125
T-95-3	300	0	100	-	-	-	107	135	0.127
T-95-4	293	2.5	97.5	-	-	-	109	133	0.117
T-95-5	300	5	95	-	-	-	103	129	0.119
T-95-6	300	10	90	-	-	-	102	128	0.101
T-95-7	300	15	85	-	-	-	106	130	0.109
T-95-8	300	25	75	-	-	-	96,	120	0.119
T-95-9	300	25	75	-	-	-	110	131	0.122
Avg	300	25	75				103	125	0.121
T-95-10	300	40	60	-	-	-	109	136	0.120

YS = Yield Strength, UTS = Ultimate Tensile Strength, and PSF = Plastic Strain to Failure

Table 4.2: Mechanical properties of C-110 specimens after SSC test

No.	H2S (ppm)	CO_2 (%)	CH_4 (%)	Before Exposure			After Exposure		
				YS, kpsi	UTS, kpsi	PSF	YS, kpsi	UTS, kpsi	PSF
C-110-1	0	0	100	-	-	-	110	133	0.034
C-110-2	-	-	-	118	136	0.036	-	-	-
C-110-3	300	0	100	-	-	-	116	143	0.05
C-110-4	293	2.5	97.5	-	-	-	105	122	0.035
C-110-5	285	5	95	-	-	-	106	118	0.022
C-110-6	270	10	90	-	-	-	-		0
C-110-7	270	10	90	-	-	-	108	128	0.057
C-110-8	270	10	90	-	-	-	-		0
Avg	270	10	90				108	128	0.019
C-110-9	255	15	85	-	-	-	104	118	0.013
C-110-10	255	15	85	-	-	-	108	123	0.032
Avg	255	15	85				106	120	0.023
C-110-11	300	25	75	-	-	-	103	122	0.056
C-110-12	300	25	75	-	-	-	112	122	0.015
Avg	300	25	75				107	122	0.035
C-110-13	300	40	60	-	-	-	117	143	0.103
C-110-14	300	40	60	-	-	-	-	n/a	0
Avg	300	40	60				117	143	0.051

Measurements of Test No. 1 through 11 of C-110 are obtained from Tale (2014).
YS = Yield Strength, UTS = Ultimate Tensile Strength, and PSF = Plastic Strain to Failure

Table 4.3: Mechanical properties of Q-125 specimens after SSC test

No.	H2S (ppm)	CO_2 (%)	CH_4 (%)	Before Exposure			After Exposure		
				YS, kpsi	UTS, kpsi	PSF	YS, kpsi	UTS, kpsi	PSF
Q-125-1	-	-	-	146	172	0.069	-	-	-
Q-125-2	0	0	100	-	-	-	153	176	0.075
Q-125-3	300	0	100	-	-	-	153	174	0.079
Q-125-4	293	2.5	97.5	-	-	-	151	174	0.061
Q-125-5	300	5	95	-	-	-	145	165	0.046
Q-125-6	300	10	90	-	-	-	135	158	0.028
Q-125-7	300	15	85	-	-	-	141	165	0.047
Q-125-8	300	25	75	-	-	-	-		0
Q-125-9	300	25	75	-	-	-	125	134	0.007
Avg	300	25	75				125	134	0.003
Q-125-10	300	40	60	-	-	-	145	171	0.058

YS = Yield Strength, UTS = Ultimate Tensile Strength, and PSF = Plastic Strain to Failure

4.2 Failure Analysis

Specimen failure behavior is analyzed by examining stress – strain profile of an exposed sample together with its crack characteristics obtained from a digital microscope.

4.2.1 Stress – Strain Profile

The true stress-strain plots are analyzed by excluding the sensor dead zone (stress level of less than 20,000 psi) in which the transducer fails to detect the elevation change. Specimen C-110-1 did not rupture in SSC cell during 15-day exposure, which demonstrates suitability of both the cell and C-110 minipipe for conducting SSC corrosion experiments. The specimen was strained to failure in TST apparatus after recovering from the cell (Fig. 4.2a). The result shows ductile failure, indicating plastic type deformation. Figure 4.2b presents stress-strain plot of C-110-2 (baseline specimen). Mechanical properties of Specimen C-110-1 are not significantly different from the values of the baseline specimen (C-110-2), confirming absence of embrittlement after exposure.

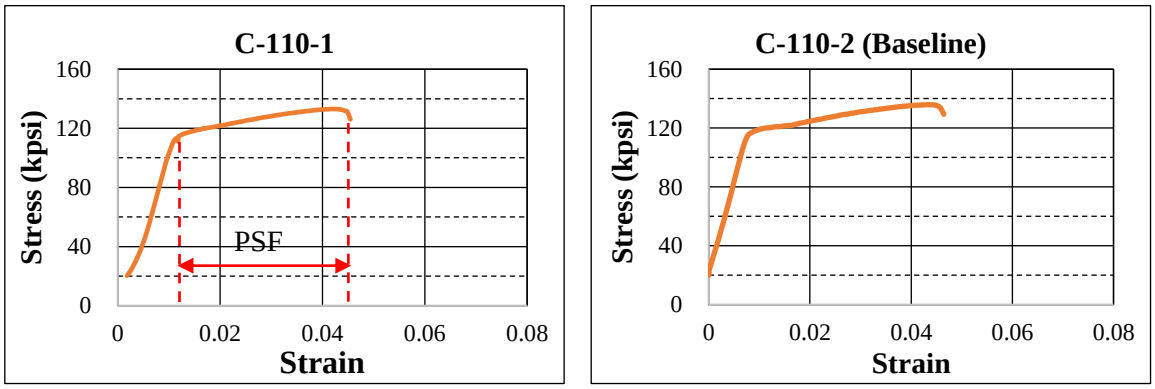


Figure 4.2: Stress-Strain profiles: a) C-110-1; and b) C-110-2 (baseline)

T-95 and Q-125 minipipes (T-95-2 and Q-125-2) were also used to verify pressure holding capacities of the corrosion cell and minipipes. The specimens did not fail in SSC cell during the test, which confirms suitability of the minipipes for the SSC experiment. Figures 4.3 and 4.4 display the stress-strain diagrams of baseline specimens (T-95-1 and Q-125-1) and specimens used during pressure testing (T-95-2 and Q-125-2). As expected, results indicate no embrittlement after the pressure test.

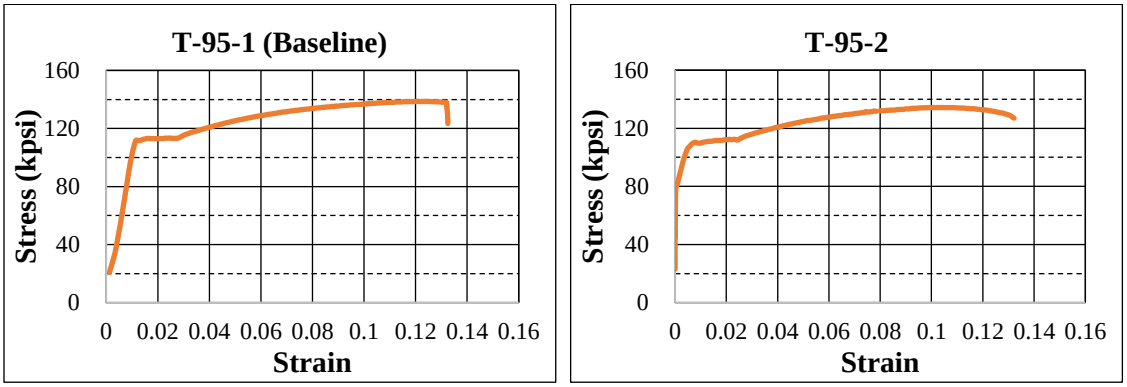
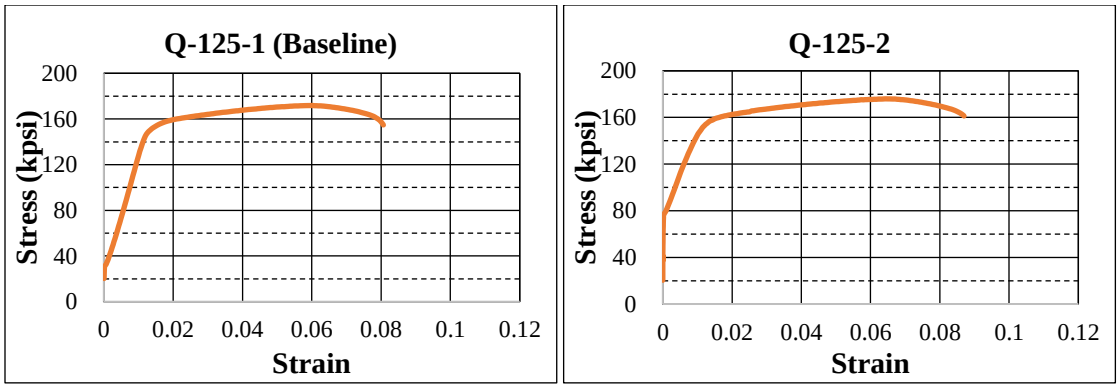


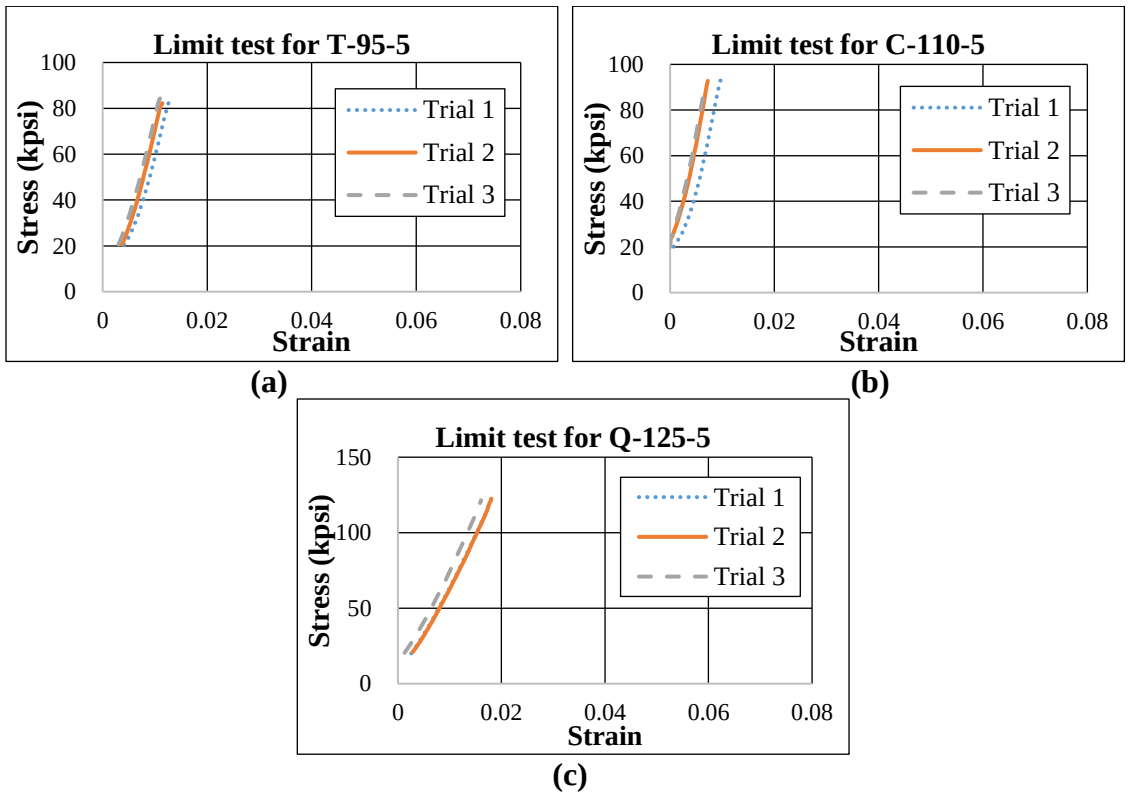
Figure 4.3: Stress-strain profiles: a) T-95-1 (baseline); and b) T-95-2



(a) (b)

Figure 4.4: Stress-strain profiles: a) Q-125-1 (baseline); and b) Q-125-2

As described in Chapter 3, limit test was performed on all specimens before and after exposure to the corrosive environment. Three limit tests were made to ensure the elasticity of the specimen and absence of inherent crack. Figure 4.5 shows stress-strain data of Specimen T-95-5, C-110-5 and Q-125-5 during limit tests. The three trial plots do not show substantial difference.



(a) (b)

(c)

Figure 4.5: Stress-strain profiles of limit test specimens: a) T-95-5; b) C-110-5; and c) Q-125-5

Specimen T-95-3, C-110-3 and Q-125-3 were tested without presence of CO_2 in the corrosion environment. Thus, the stress-strain measurements in Fig. 4.6 indicate impact of H_2S on mechanical property of specimens in absence of CO_2. The specimens did not fail during the SSC test, hence TST apparatus was utilized to strain them until failure. As depicted in stress-strain curves and UTS and PSF values of the specimens (Tables 4.1 to 4.3), results show no sign of embrittlement. PSF of the specimens increased from the baseline values. UTS of T-95-3 is slightly reduced after exposure; however, the difference is negligible to consider the occurrence of embrittlement.

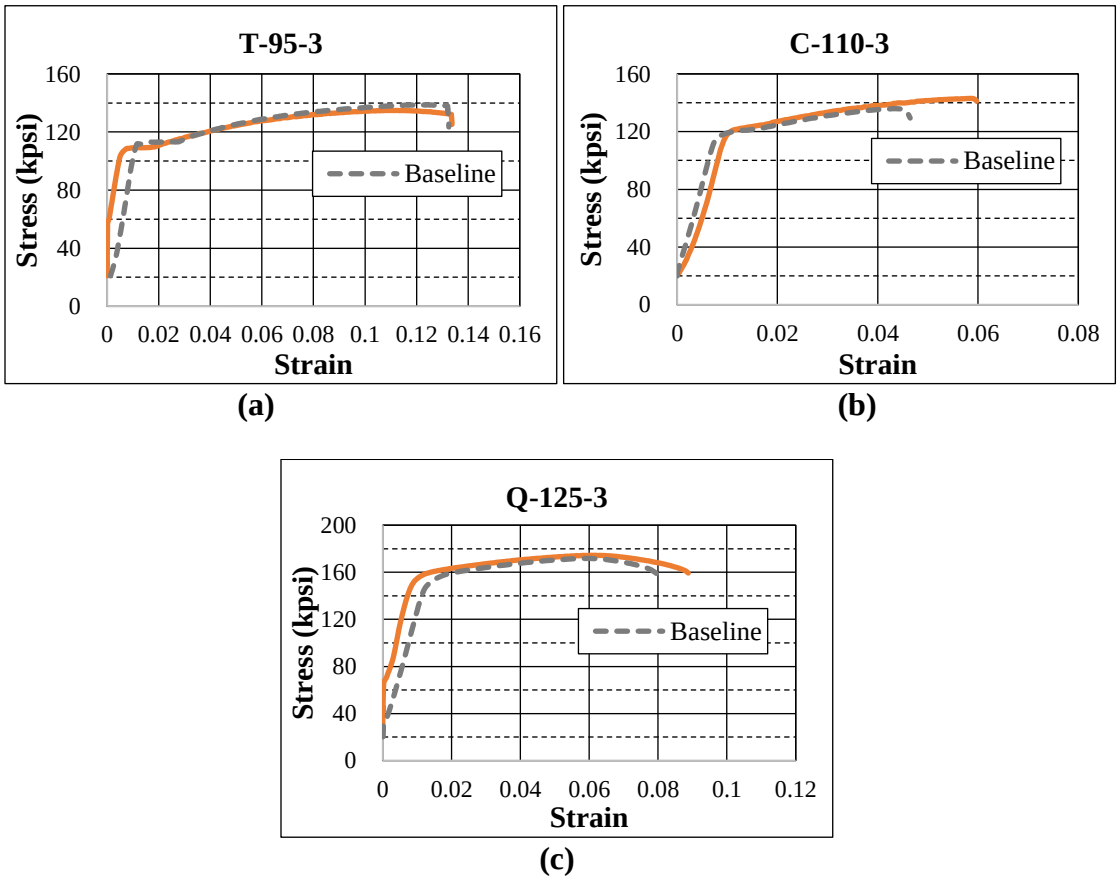


Figure 4.6: Stress-Strain profiles: a) T-95-3; b) C-110-3; and c) Q-125-3

Specimen T-95-4, C-110-4 and Q-125-4 were also exposed to 2% NaCl solution saturated with mixed gas containing approximately 97.5% methane, 2.5% of

CO_2 and 300 ppm H_2S (Fig. 4.7). None of the samples fail during the SSC test; however, they demonstrated partial embrittlement due to presence of small amount of H_2S. Compared to baseline values, PSF of the specimens considerably decreased while there UTS displayed some level of reduction except for Q-125-4. Even though the UTS of Q-125-4 shows slight reduction when compared to Q-125-3, it remained almost identical to the value of baseline specimen (Q-125-1).

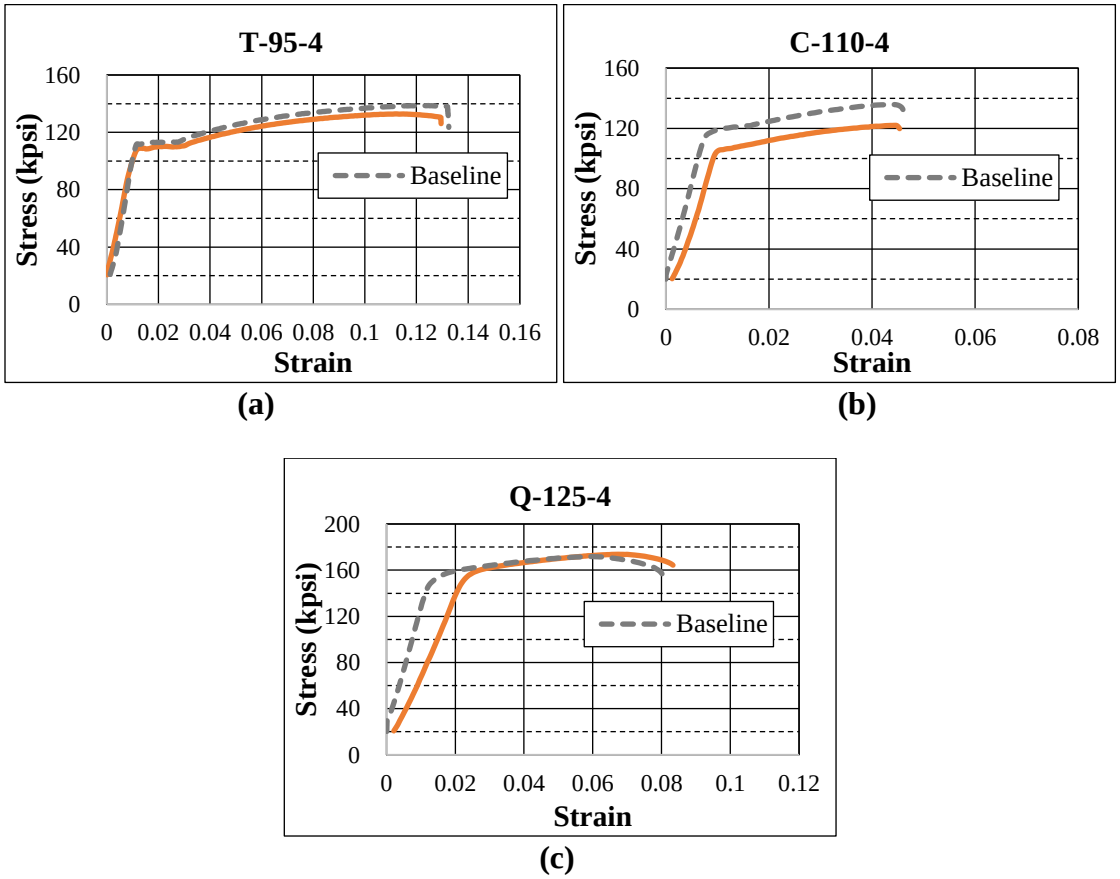


Figure 4.7: Stress-strain profiles of specimens exposed to corrosive environment containing 2.5% CO_2: a) T-95-4; b) C-110-4; and c) Q-125-4

Specimens T-95-5, C-110-5 and Q-125-5 were tested at 5% CO_2 concentration in the corrosive environment. Stress-strain curves presented in Fig. 4.8 show mechanical property (PSF and UTS) changes resulting from exposure to the corrosive environment. As indicated by reduction in PSF (i.e. reduction in ductility), results

demonstrate considerable embrittlement after exposure. Nonetheless, the specimens endured the 7 days exposure to sulfide stress cracking environment without fracture.

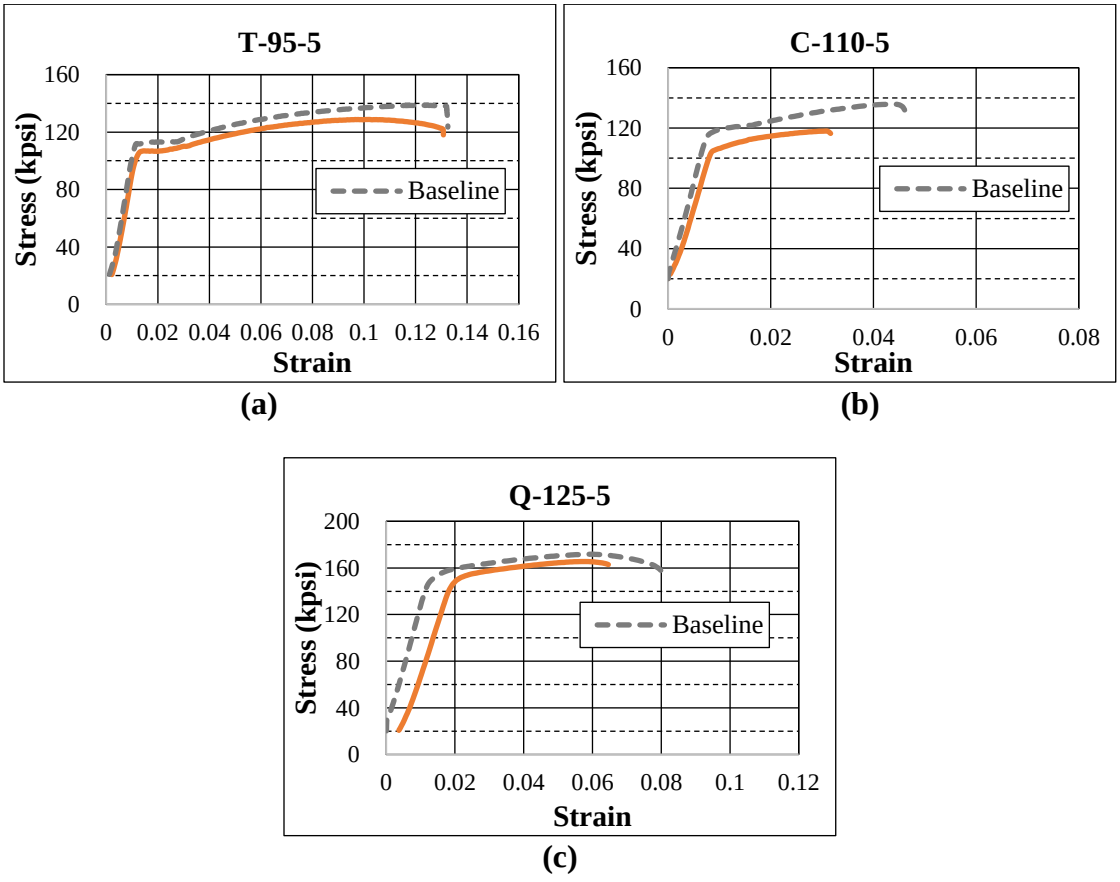


Figure 4.8: Stress-strain profiles of specimens exposed to corrosive environment containing 5% CO_2: a) T-95-5; b) C-110-5; and c) Q-125- 5

In order to capture the trend PSF and UTS, CO_2 concentration was increased to 10% during the investigation. Tests were performed using Specimens T-95-6, C-110-6 and Q-125-6. As indicated by reduction in PSF of T-95-6 and Q-125-6, the embrittlement further increased with CO_2 concentration (Fig. 4.9). UTS also reduced significantly after exposure. Moreover, visual examination shown in Fig. 4.10 indicated brittle failure as demonstrated by very sharp breaking of the specimen without showing some form of necking. When ductile failure occurs, specimens often show noticeable necking at the breaking point. Specimen C-110-6 was broken inside the

SSC cell on the seventh day of testing. This indicates presence of severe sulfide stress cracking and embrittlement. Although the failure indicates presence of embrittlement, identical SSC tests were conducted on two specimens (C-110-7 and C-110-8) to validate the result obtained from Specimen C-110-6. However, Specimen C-110-7 did not show signs of embrittlement. Specimen C-110-8 was also broken on the seventh day of exposure to the corrosive environment while carrying tensile load, which produces stress level of 80% of its yield strength. In order to quantify the mechanical properties of the specimen after exposure, average UTS and PSF values of Specimen C-110-6, C-110-7 and C-110-8, are considered. Both average values are less than those of baseline specimen, indicating strong embrittlement. Therefore, the increase in CO_2 concentration exacerbates the sulfide stress cracking and related embrittlement.

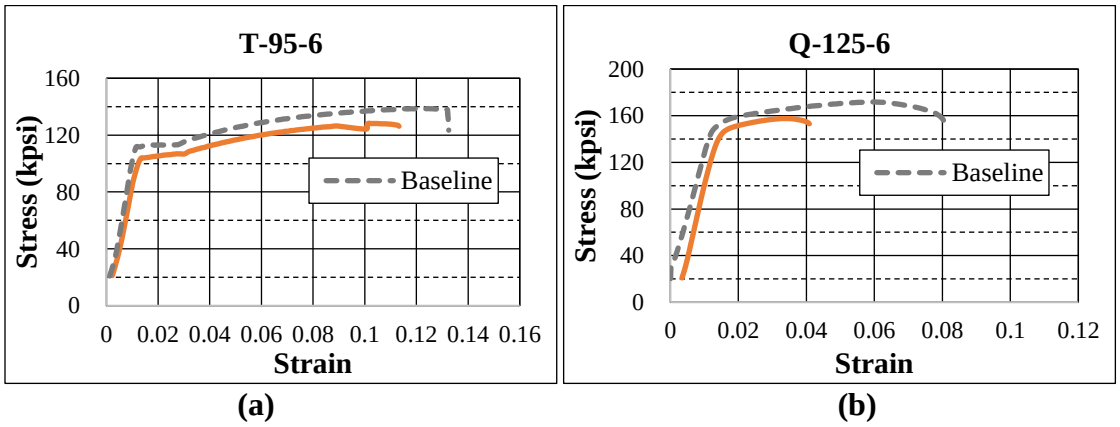


Figure 4.9: Stress-strain profiles of specimens exposed to corrosive environment containing 10% CO_2: a) T-95-6; and b) Q-125-6

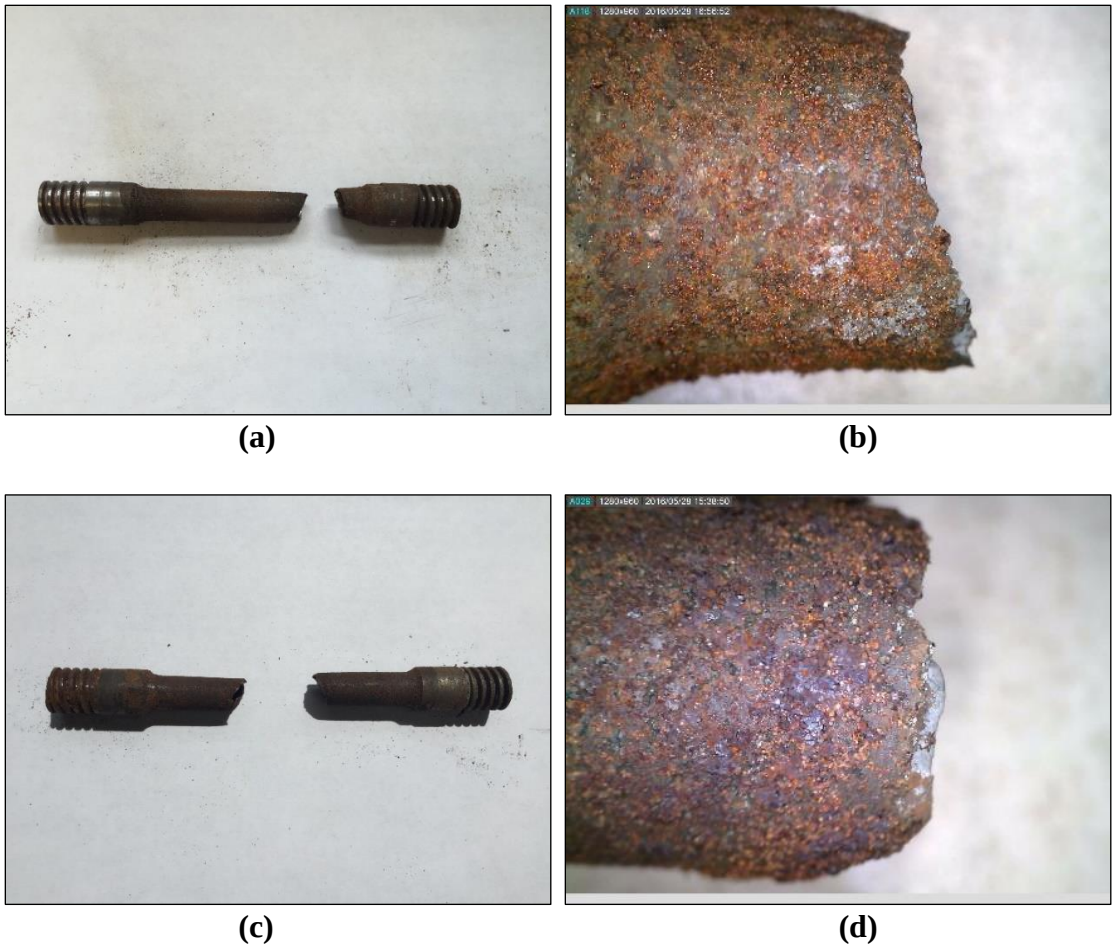


Figure 4.10: Schematic of failure of specimens exposed to corrosive environment containing 10% CO_2: a) Front view of T-95-6; b) Microscopic view of T-95-6; c) Front view of Q-125-6; and d) Microscopic view of Q-125-6

Specimens T-95-7, Q-125-7, C-110-9 and C-110-10 were tested at increased CO_2 concentration (15%). Specimen C-110-10 was used for a repeat test, which was conducted to check the PSF value obtained from C-110-9. The average value of Specimen C-110-9 and C-110-10 is used in analysis. The specimens from different steel grades exhibited embrittlement behavior as indicated by the reduction of UTS and PSF (Fig. 4.11).

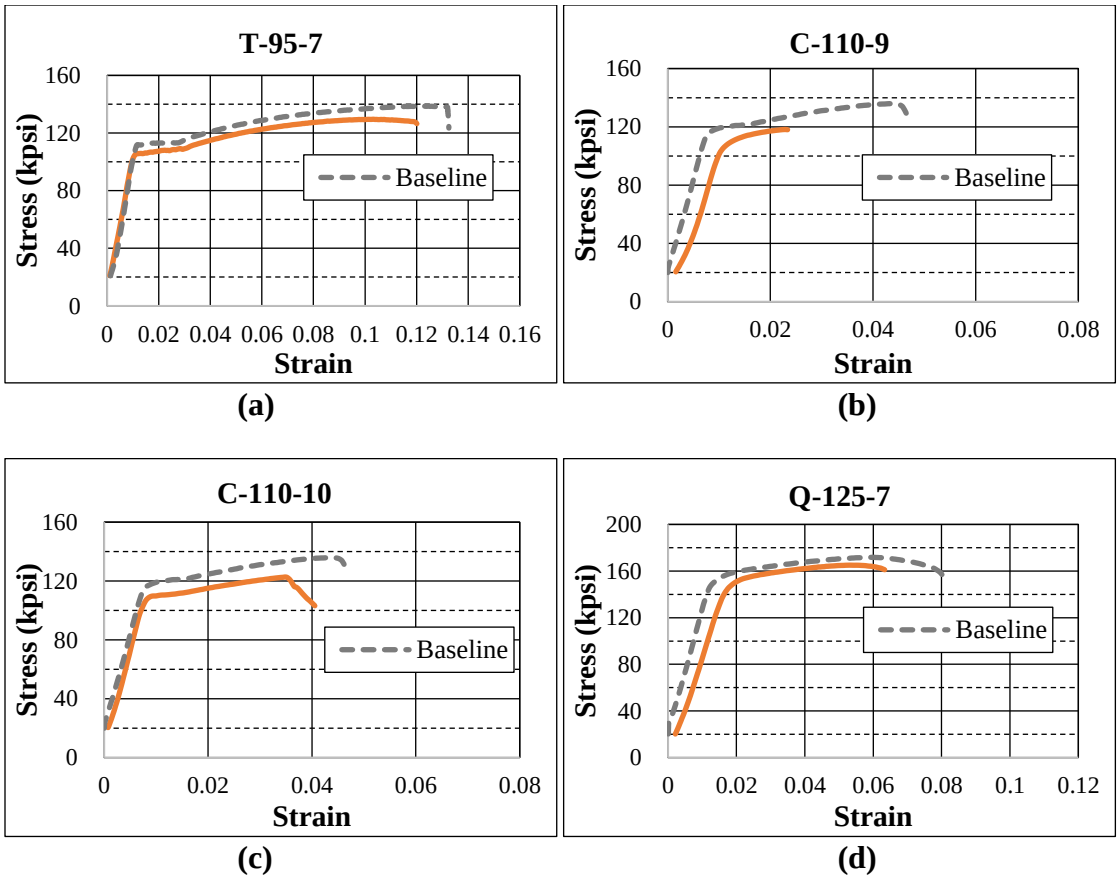


Figure 4.11: Stress-strain profiles of specimens exposed to corrosive environment containing 15% CO_2: a) T-95-7; b) C-110-9; c) C-110-10; and d) Q-125-7

Furthermore, repeated (twice) SSC tests were performed at higher CO_2 concentration (25% CO_2). Results (Fig. 4.12) show occurrence of embrittlement in some of the specimens tested. Specimens T-95-8 and T-95-9 did not fail in the SSC cell. Their average mechanical properties show embrittlement behavior since UTS and PSF were less than baseline specimen. For C-110, the SSC tests were repeated after Specimen C-110-11 displayed unexpected PSF. For the two specimens, the average UTS and PSF measurements were obtained. The results showed embrittlement fracture. Unlike T-95 and C-110, the first trial of Q-125 (Specimen Q-125-8), failed on the seventh day of the SSC test. The test was repeated and the specimen tolerated the tensile load without rupturing. However, the aged sample broke shortly during the

complete strength test, which provided low values of UTS and PSF. As a result, the average UTS and PSF of Specimens Q-125-8 and Q-125-9 are significantly low indicating substantial embrittlement after exposure.

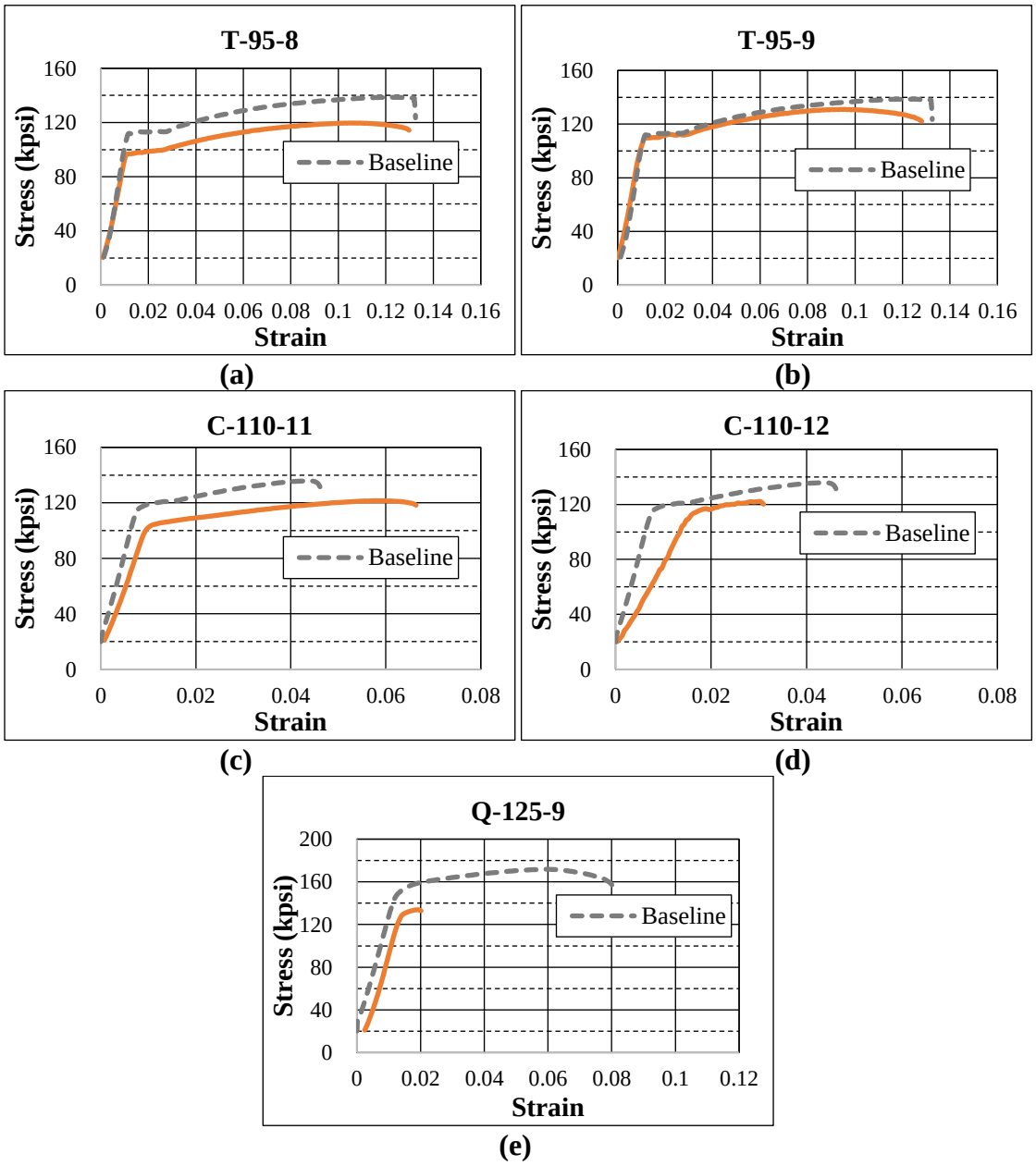


Figure 4.12: Stress–strain profiles of specimens exposed to corrosive environment containing 25% CO_2: a) T-95-8; b) T-95-9; c) C-110-11; d) C-110-12; and e) Q-125-9

The last batch of SSC tests conducted on the API carbon steels were performed at CO_2 concentration of 40%. Results (Fig. 4.13) show moderate reduction of UTS and PSF of T-95-10 as a result of partial embrittlement. Specimen C-110-13 showed unexpected high UTS and PSF when tested at 40% CO_2. The test was repeated using Specimen C-110-14, which results in early failure after four days of exposure to the corrosive environment. The average UTS and PSF values do not show embrittlement. Unlike C-110, Specimen Q-125-10 demonstrated brittle failure behavior after exposure to the corrosive environment.

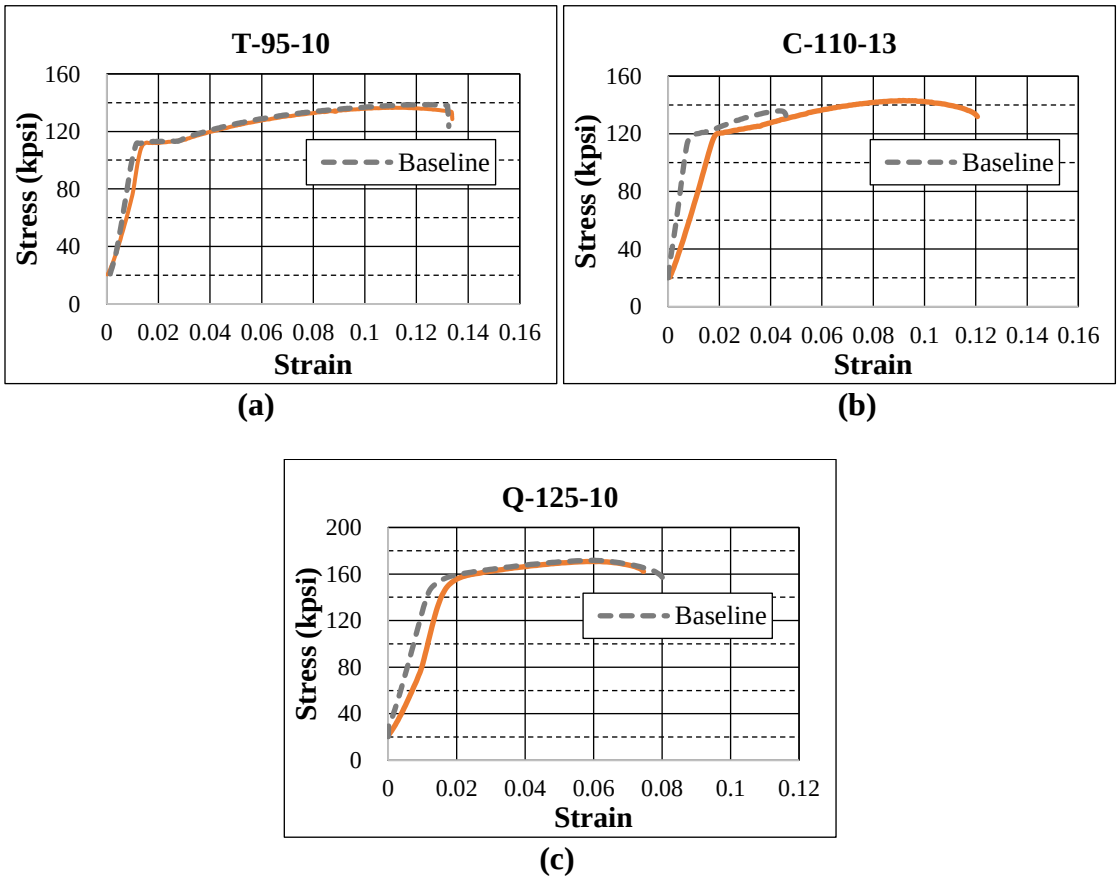
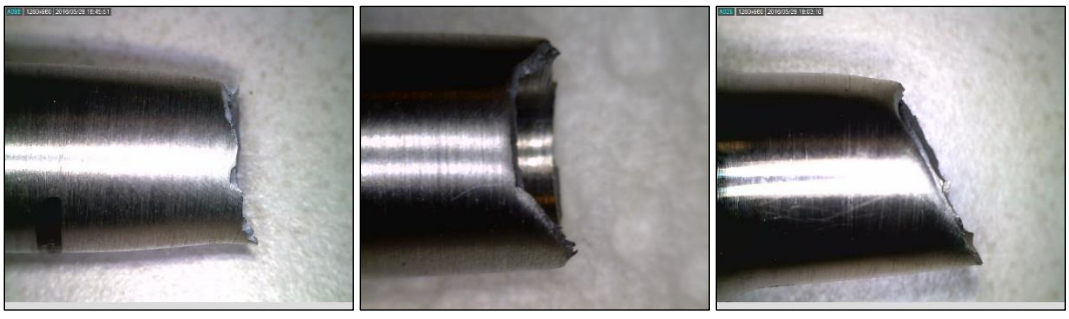


Figure 4.13: Stress–strain profiles of specimens exposed to corrosive environment containing 40% CO_2: a) T-95-10; b) C-110-13; and c) Q-125-10

4.2.2 Crack Features

To augment measurements obtained from the TST test, cracks of the specimens after complete strength test were examined using a digital microscope. Ductile failure involves extensive plastic deformation before rupturing, in which crack propagates slowly by shear deformation near separation region. The delay in development of crack makes the specimen strained axially with stable neck and creates a fibrous fracture cross-section. During brittle failure, crack propagation happens rapidly, resulting in relatively small plastic deformation and non-fibrous cutting-edge, which is nearly perpendicular to the direction of the tensile stress. (Zhigilei 2010)

As expected from clean metallic materials, baseline specimens of T-95, C-110 and Q-125 show precise ductile failure characteristics with necking and fibrous region around the crack (Fig. 4.14). Specimens used in the pressure holding test also show ductile type failure (Fig. 4.15). Specimens exposed to the corrosion environment in absence of CO_2 also did not show brittle type of failure (Fig. 4.16). The fracture characteristics indicates ductile type failure with necking and fibrous crack region. Results from microscopic image analysis are predominately in agreement with stress-strain measurements.



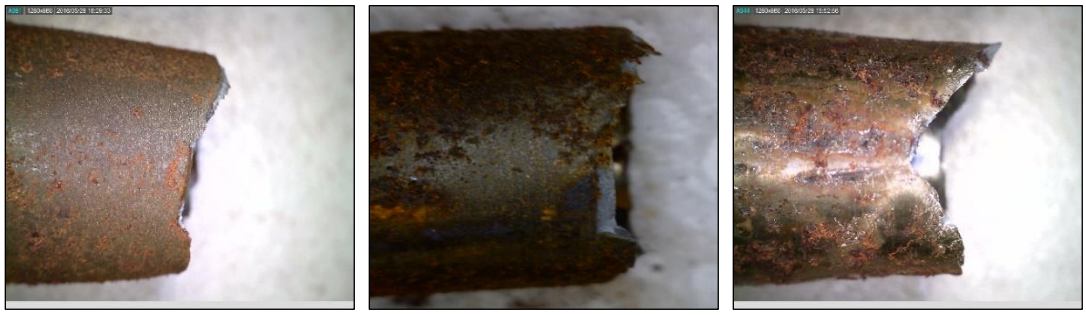
(a) **(b)** **(c)**

Figure 4.14: Crack features of baseline specimens: a) T-95-1; b) C-110-2; and c) Q-125-1



(a) (b) (c)

Figure 4.15: Crack features of specimens used in pressure holding tests: a) T-95-2; b) C-110-1; and c) Q-125-2



(a) (b) (c)

Figure 4.16: Crack features of specimens exposed to the corrosion environment in absence of CO_2: a) T-95-3; b) C-110-3; and c) Q-125-3

Initially ductile specimens became brittle when exposed to the corrosion environment containing 2.5% CO_2 during the SSC testing. When CO_2 concentration was 2.5%, the characteristics of embrittlement were observed as indicated by development of sharp fracture edges (Figs. 4.17a and 4.17b) that are perpendicular to the direction of the tensile force. Microscopic images presented in Fig. 4.17c display fracture characteristics Q-125 grade which exhibits certain level of ductility. Mostly, outcomes of fracture feature analysis are in agreement with stress-strain measurements.



(a) **(b)** **(c)**

Figure 4.17: Crack features of specimens exposed to the corrosion environment containing 2.5% CO_2: a) T-95-4; b) C-110-4; and c) Q-125-4

Figure 4.18 presents crack features of specimens exposed to the corrosion environment containing 5% CO_2 during the SSC testing. The shear deformation with necking and fibrous cracks were not observed, indicating presence of strong brittle failure as exhibited in stress–strain plot analysis.



(a) **(b)** **(c)**

Figure 4.18: Crack features of specimens exposed to the corrosion environment containing 5% CO_2: a) T-95-5; b) C-110-5; and c) Q-125-5

Apart from the microscopic comparison, pictures of Specimens Q-125-5 and Q-125-1 (baseline) were obtained and compared (Fig. 4.19) to show features of brittle and ductile failures during shear formation. The embrittled specimen (Q-125-5) displayed necking and fibrous fracture, which is perpendicular to the tensile force direction.



(a) **(b)**

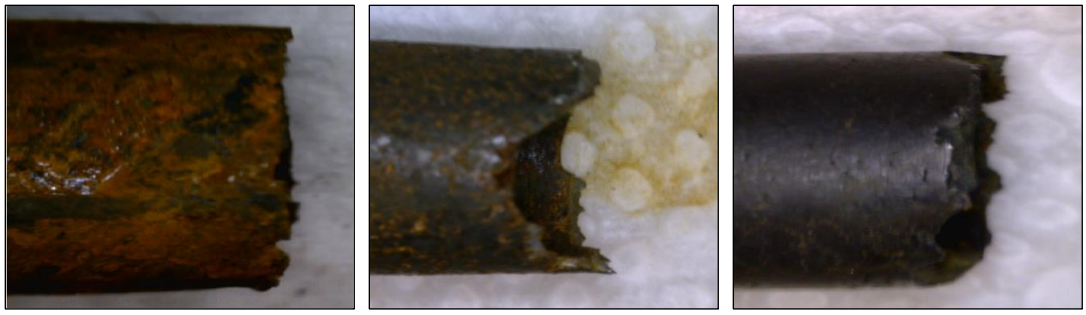
Figure 4.19: Comparison of features of brittle and ductile failures: a) Q-125-5; and b) Q-125-1 (baseline)

After exposure to the corrosive environment containing 10% CO_2 concentration in the SSC test cell, T-95 and Q-125 exhibited fairly brittle characteristics with fibrous fracture tips (Fig. 4.20). Mechanical properties (UTS and PSF) also indicate brittle failure. C-110 exhibits the maximum brittleness at 10% CO_2 concentration, as the specimens failed twice during the SSC test out of three trials. The UTS and PSF measurements are consistent with fracture characteristic analysis (Fig. 4.21). Microscopic image analysis (Fig. 4.22) of Specimens T-95-7, C-110-9, C-110-10 and Q-125-5 shows considerable embrittlement after SSC test, which was conducted in corrosive environment containing 15% CO_2.



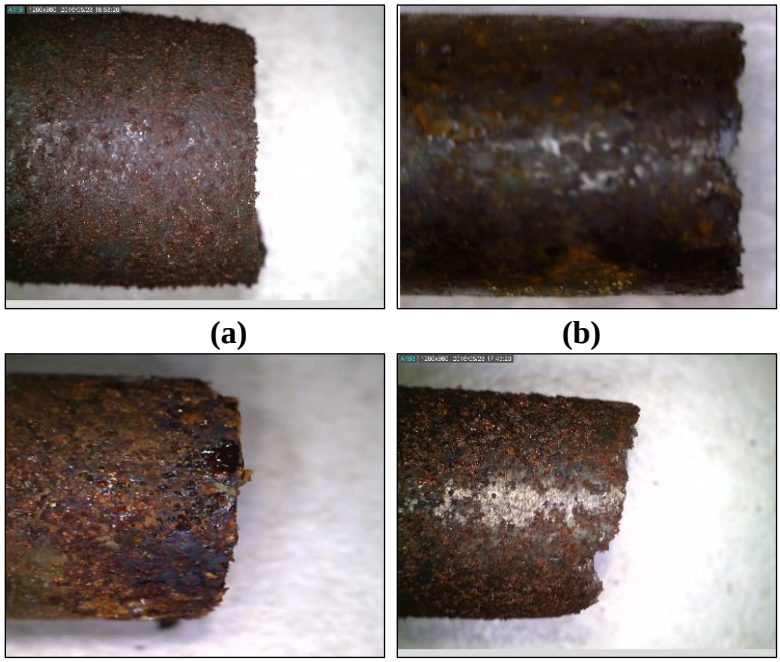
(a) **(b)**

Figure 4.20: Crack features of specimens exposed to the corrosive environment containing 10% CO_2 concentration: a) T-95-6; and b) Q-125-6



(a) **(b)** **(c)**

Figure 4.21: Crack features of C-110 specimens exposed to the corrosive environment containing 10% CO_2 concentration: a) C-110-6; b) C-110-7; and c) C-110-8



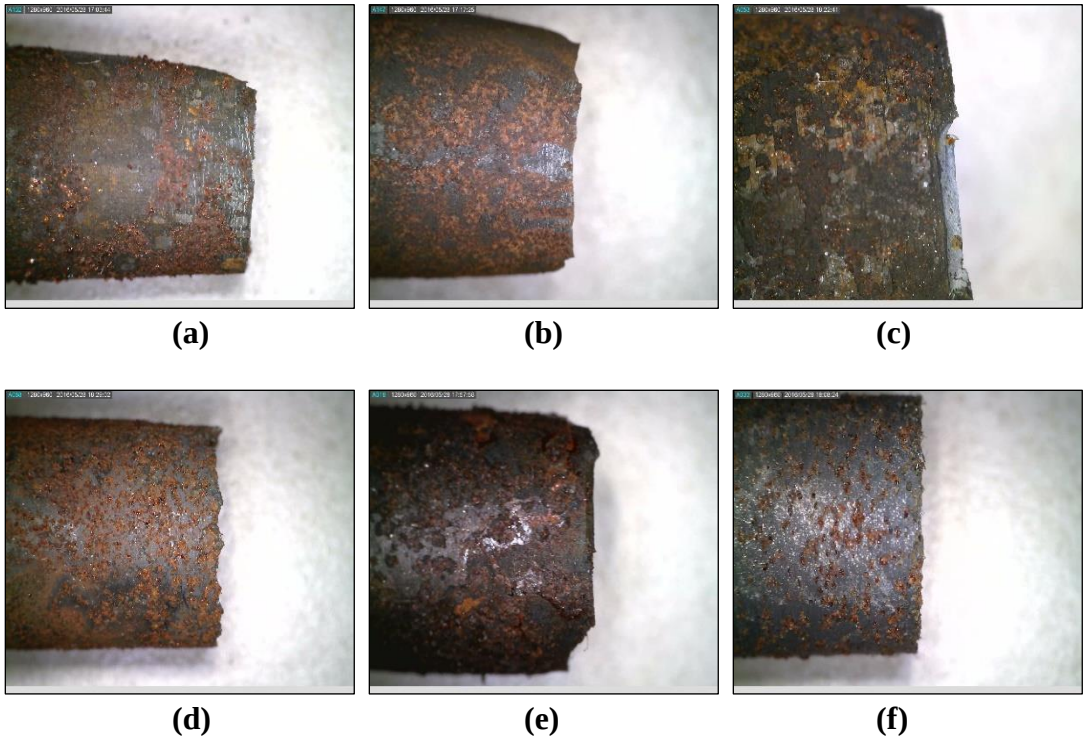
(a) **(b)**

(c) **(d)**

Figure 4.22: Crack features of specimens exposed to the corrosive environment containing 15% CO_2 concentration: a) T-95-7; b) C-110-9; c) C-110-10 (repeated test); and d) Q-125-5

As indicated by the fracture features, T-95 and C-110 specimens (Fig. 4.23) showed partial embrittlement when tested in corrosion environment containing 25% CO_2. When tested under similar condition, Q-125 specimens displayed severe embrittlement as demonstrated by specimen failure during the SSC test and brittle type

specimen failure during TST test, which showed almost no plastic deformation (i.e. approximately zero PSF). Microscopic images presented in Figs. 4.23e and 4.23f show brittle type failure without fibrous tips and fracture edges that are perpendicular to the tensile force direction.



(a) **(b)** **(c)**

(d) **(e)** **(f)**

Figure 4.23: Crack features of specimens exposed to the corrosive environment containing 25% CO_2 concentration: a) T-95-8; b) T-95-9; c) C-110-11;d) C-110-12; e) Q-125-8; and f) Q-125-9

Figure 4.24 displays the results of the last experiment conducted at the highest CO_2 concentration (40%). As depicted in stress–strain curve with mechanical property changes, T-95 showed brittle failure. Two C-110 specimens were tested and they displayed inconsistent stress–strain curves, one specimen showing brittleness and another one exhibiting good ductility. This has complicated the determination of failure type at this CO_2 concentration. The first C-110 specimen (C-110-13) displayed ductile failure when tested with TST apparatus; however, microscopic investigation of

the broken specimen fracture tips (Fig. 4.24) indicates brittle failure. The second specimen showed severe brittle fracture since it failed after four days of exposure to corrosive environment. The discrepancies can be attributed to variation in SSC susceptibility resulting from manufacturing defects. Crack features of Q-125 specimen also exhibited abnormal behavior which is not consistent with mechanical property measurements, which indicate slight embrittlement while the microscopic evidence suggests ductile type failure with considerable features of shear deformation.

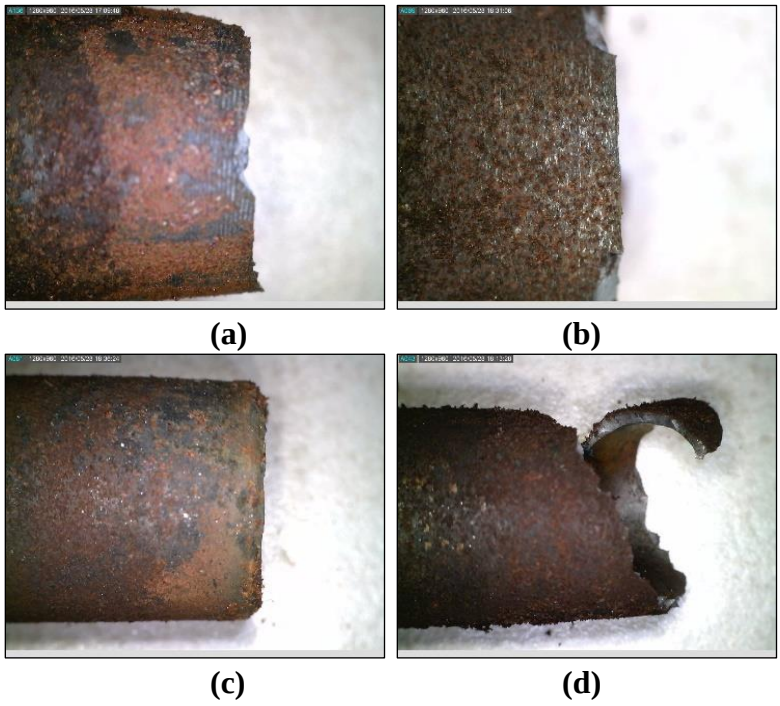


Figure 4.24: Crack features of specimens exposed to the corrosive environment containing 40% CO_2 concentration: a) T-95-10; b) C-110-13; c) C-110-14; and d) Q-125-10

4.3 Effect of CO_2

In Sections 4.1 and 4.2, the impact of CO_2 concentration on SSC susceptibility is examined considering UTS and PSF values. Stress–strain profiles indicate the change in mechanical properties occurring after exposure to the corrosive environment

in the SSC test cell. Figures 4.25 and 4.26 present UTS and PSF of exposed and baseline specimens as a function of CO_2 concentration. To generate the plots, average values of UTS and PSF were used for repeated experiments. UTS and PSF for all the steel grades tend to decrease until a critical CO_2 concentration, which can be between 10 to 30%. The decrease in UTS and PSF indicates loss of strength and ductility demonstrating increase in SSC susceptibility. Above the critical concentration, the trend reverses and the resistance to SSC improves with CO_2 concentration. T-95 and C-110 exhibited roughly the same PSF at low (≈0%) and high (40%) CO_2 concentrations. For T-95 steel, the difference between PSF of baseline specimens and that of exposed specimens are minimal. These differences are significant for C-110 and Q-125, which are expected to be more susceptible than T-95 due to their high strength.

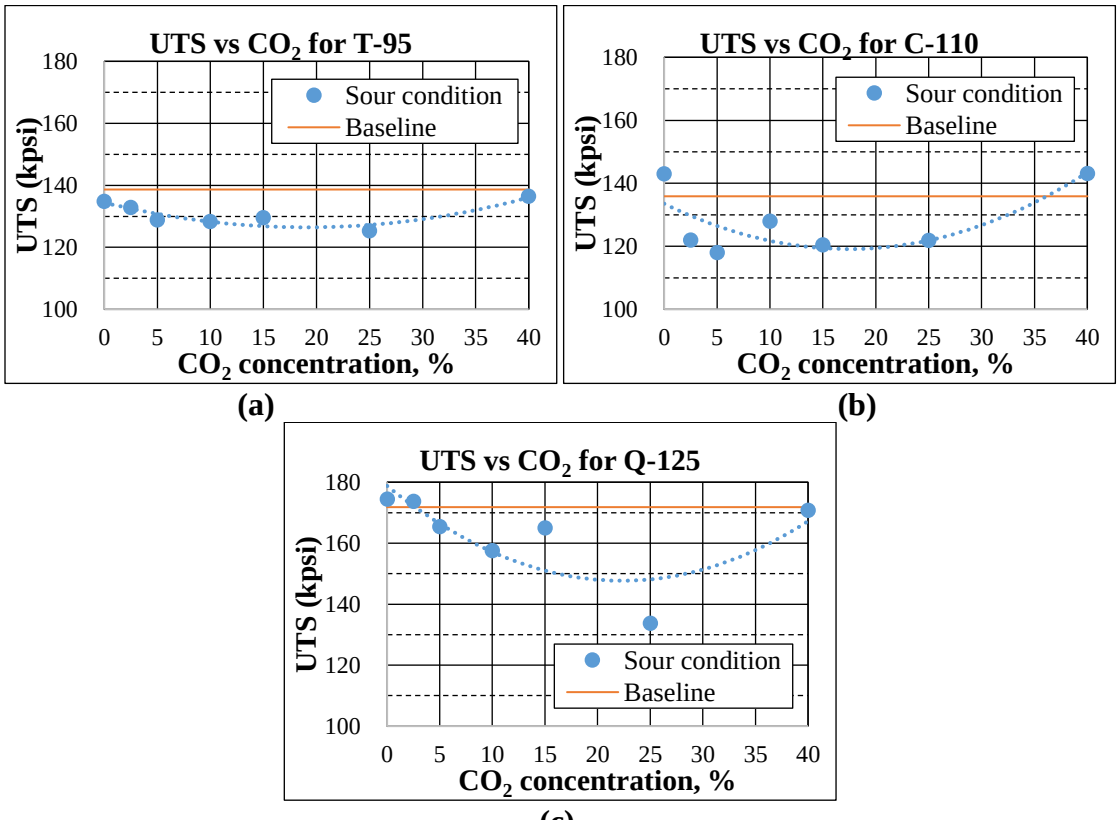


Figure 4.25: Ultimate tensile strength vs. CO_2 concentration: a) T-95; b) C-110; and c) Q-125

Exposed and baseline specimens of Q-125 displays the highest differences in values of UTS and PSF. The UTS and PSF values drastically diminish when CO_2 concentration was maintained between 15 and 40%. The critical concentration is approximately 25% for this steel grade. Hence, Q-125 is the most susceptible grade to SSC in this CO_2 concentration range. Possible explanations to the concave trends of UTS and PSF profiles can be deduced by considering uniform corrosion behavior. In wet H_2S-CO_2 sour environment, following corrosion reactions occur to produce $FeCO_3$ and FeS (Elgaddafi et al. 2016):

$$Fe + H_2CO_3 \rightarrow FeCO_3 + H_2 \tag{4.1}$$

$$Fe + H_2S \rightarrow FeS + H_2 \tag{4.2}$$

These reactions form $FeCO_3$ and FeS protective layers on the surface of exposed steel, preventing further corrosion thus decelerating the corrosion rate. Kinetics of FeS formation is known to be favorable than $FeCO_3$ formation when CO_2 and H_2S compete on the steel surface. Therefore, FeS layer is often created relatively faster than $FeCO_3$ layer and limits CO_2 corrosion (Papavinasam 2013). When H_2S content is more than 10 ppm the corrosion rate is generally expected to decrease with H_2S concentration due to the formation of FeS protective scale (Elgaddafi et al. 2015; Elgaddafi et al. 2016).

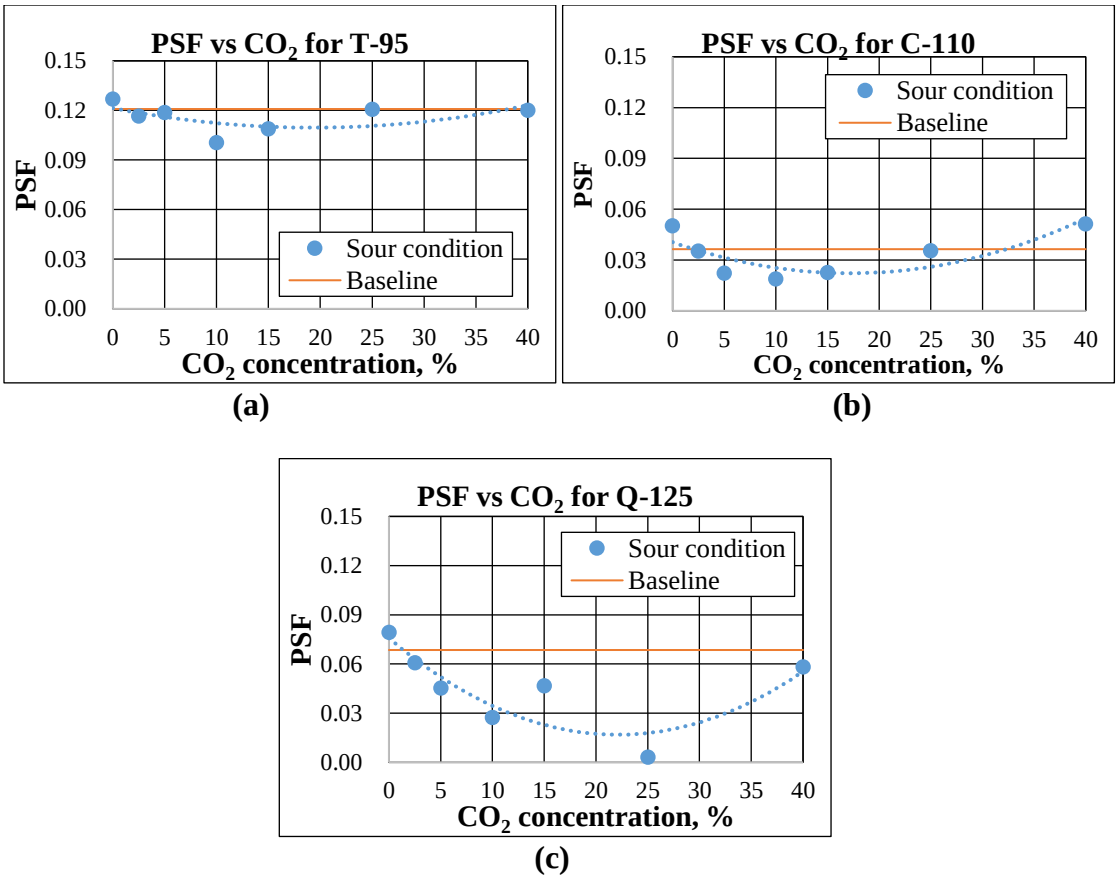


Figure 4.26: Plastic strain to failure vs. CO_2 concentration: a) T-95; b) C-110; and c) Q-125

Srinivasan and Kane (1996) described the effect of small amount of H_2S on wet H_2S-CO_2 corrosion. Presence of small amount of H_2S (i.e. ratio of pCO_2 to pH_2S greater than 200) at temperature below 120°C promotes formation of protective thin FeS film in CO_2 dominant systems. Protective film also forms in H_2S dominant system, in which the ratio of pCO_2 to pH_2S is less than 200; however, at low temperatures (lower than 60°C), H_2S presence intensifies corrosion since FeS layer becomes unstable and hinders formation of other types of protective films such as $FeCO_3$ film. The pCO_2 to pH_2S ratio of 200 approximately corresponds to 5% CO_2 concentration in this study and the test temperature was below 60°C. In this study, the stress–strain measurements show the lowest value of UTS and PSF between 10 and 30% CO_2 concentrations.

Assuming positive relationship between the corrosion rate and the mechanical properties (UTS and PSF), the film effect can be employed to explain the UTS and PSF trends against variation in CO_2 concentration.

Figures 4.27 and 4.28 present UTS and PSF measurements of T-95, C-110 and Q-125 failure tests conducted varying CO_2 concentration. Since the higher is steel grade yield strength, the more susceptibility to SSC. Therefore, PSF is expected to decrease as the strength of steel grade increases from T-95 to Q-125. In fact, Fig. 4.28 indicates that T-95 has the highest SSC resistance while C-110 shows the lowest. The possible reason for the reverse pattern between C-110 and Q-125 could be related to the chemical compositions of the steel grades. API (2005) defined typical chemical compositions of T-95, C-110 and Q-125 for sour condition as Table 4.4.

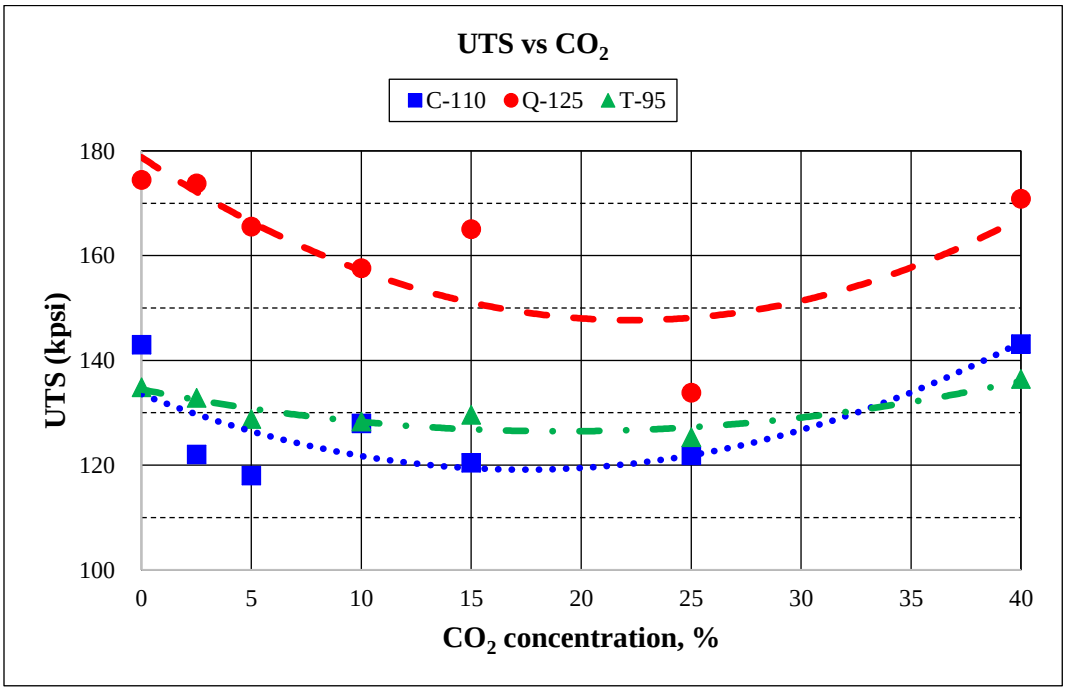


Figure 4.27: Ultimate tensile strength vs. CO_2 concentration

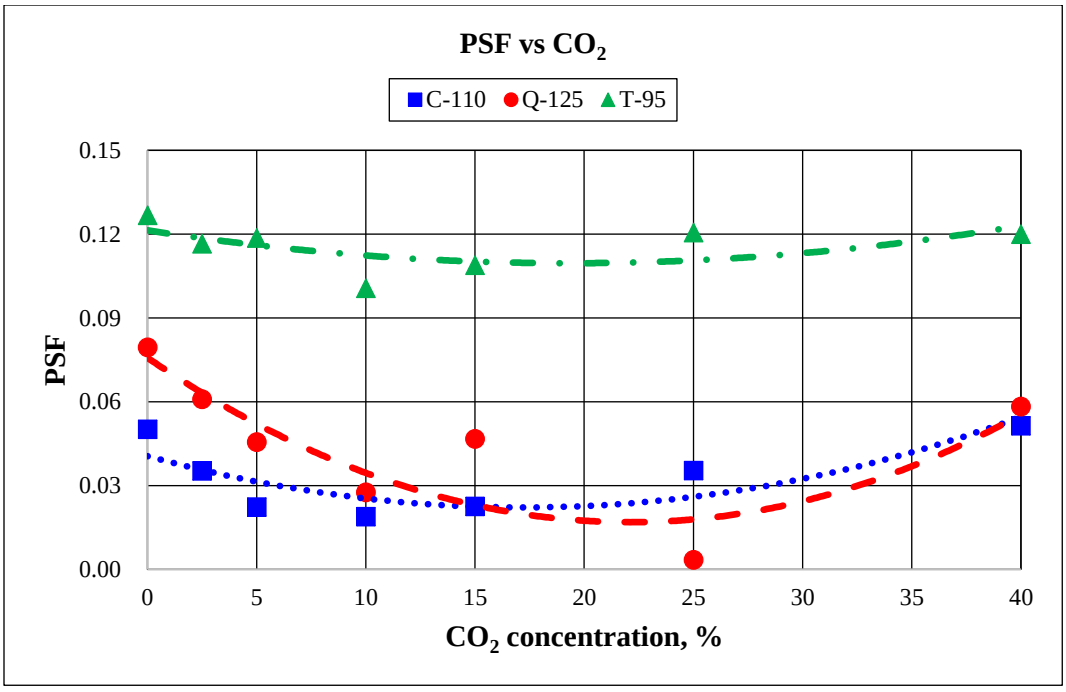


Figure 4.28: Plastic strain to failure vs. CO_2 concentration

Table 4.4: Typical chemical compositions of API carbon steels

Steel grade	Elements (Wt %)									
	C	Mn	P	S	Si	Cu	Ni	Cr	Mo	Fe
T-95	~0.35	~1.2	~0.02	~0.01	-	-	~0.99	0.4~1.5	0.25~0.85	Remainder
C-110	~0.35	~1.2	~0.02	~0.05	-	-	~0.99	0.4~1.5	0.25~1.0	Remainder
Q-125	~0.35	~1.35	~0.02	~0.01	-	-	~0.99	~1.5	~0.85	Remainder

The tested specimens' compositions (Table 3.1) fall into the API specifications. However, among the constituents listed in the Table 4.4, Nickel (Ni), Chromium (Cr) and Molybdenum (Mo) are considered to be critical factors in determining SSC resistance of steel. Ni is incorporated to improve toughness of the steels, while Cr and Mo are often used to improve oxidation resistance and hardenability, respectively (Poweleit and Monroe 2005). For the tested minipipes, Ni composition of C-110 is relatively lower than those of Q-125 and T-95. This abnormal trend may have resulted in slightly weaker SSC resistance of C-110 as demonstrated by lower PSF and UTS as

compared to Q-125. The manufacturer of C-110 is different from that of other steel grades, which resulted in unexpected compositional variation.

SSC susceptibility of a metal was analyzed by examining the reduction of baseline UTS or PSF to those of H_2S-exposed specimens. Therefore, the susceptibility trend with respect to steel grade yield strength should also be compared by normalizing the UTS and PSF changes, so that the original brittleness can be ignored. Figures 4.29 and 4.30 display the trend of dimensionless UTS and normalized PSF computed by dividing the measured UTS and PSF values of H_2S-exposed specimen by the measured UTS and PSF values of baseline specimen. Both dimensionless UTS and normalized PSF fairly well follow the anticipated sequence of nominal yield strength of tested steel grades even though there exits little deviation induced by other types of corrosion (for example, uniform corrosion) potentially presented during the test: T-95 has the highest resistance and Q-125 shows the least resistance to SSC.

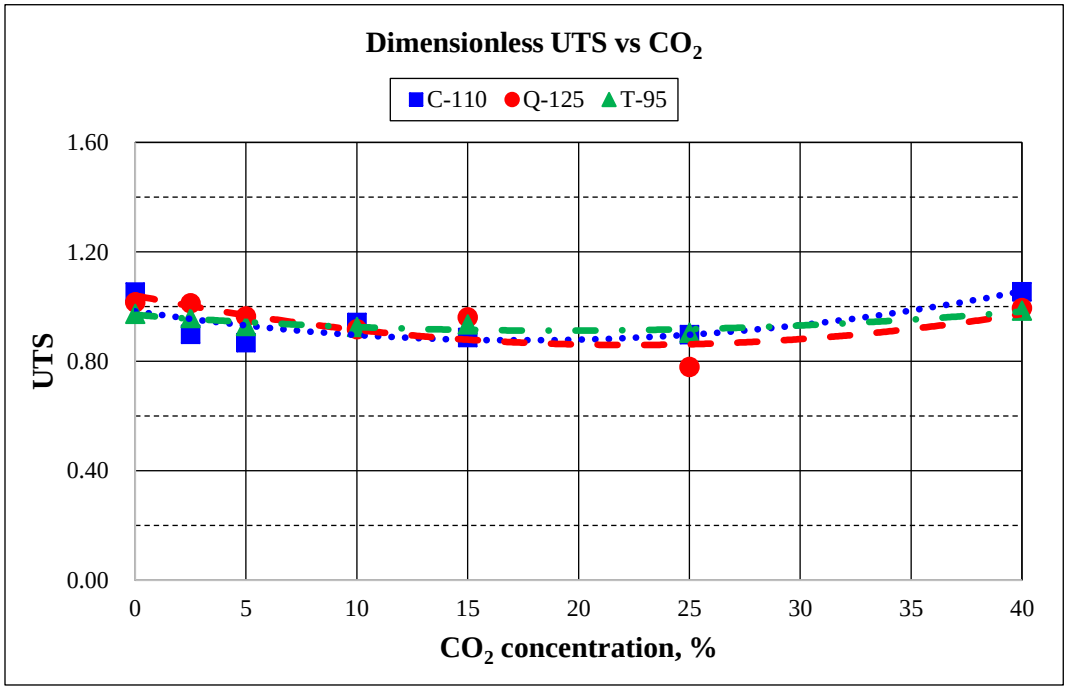


Figure 4.29: Dimensionless Ultimate tensile strength vs. CO_2 concentration

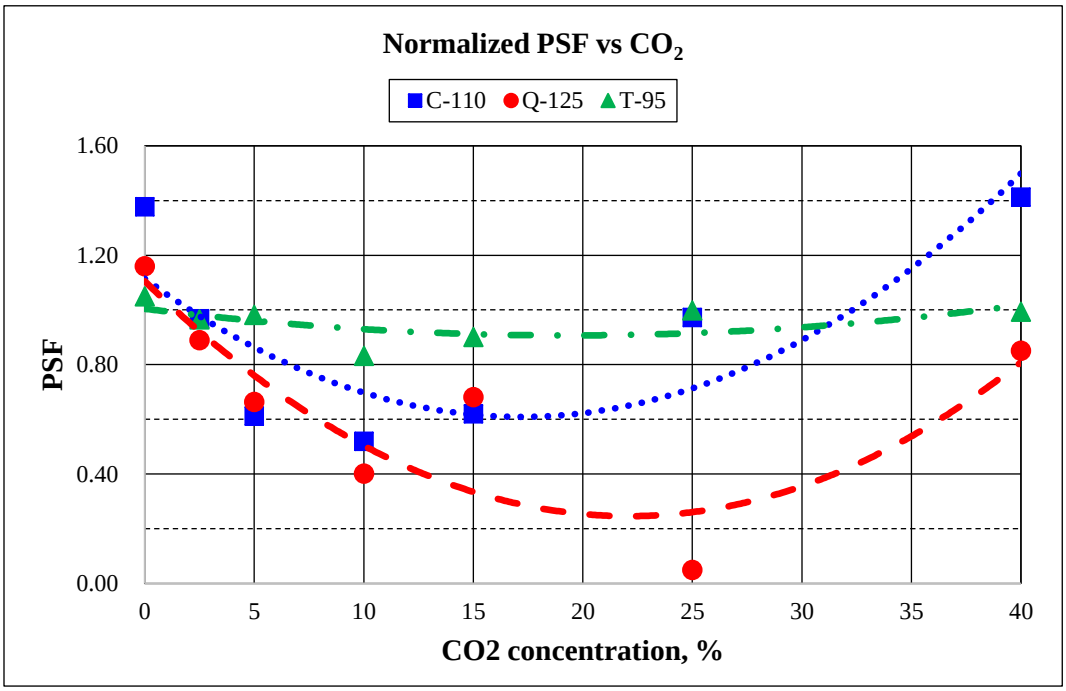


Figure 4.30: Normalized Plastic strain to failure vs. CO_2 concentration

CHAPTER 5: CONCLUSIONS AND RECOMMENDATIONS

5.1 Conclusions

Based on experimental investigation of stress cracking corrosion of API carbon steels for seven days, the following conclusions are drawn:

a. In sour environment containing brine saturated with mixed gas that has small amount of H_2S (300 ppm) and methane, pH remains nearly neutral and leaves low concentration of hydrogen ion in the solution. As a result, metal specimens maintain their ductility which is favorable in the actual failure occurrence.

b. When CO_2 concentration of the mixed gas is increased from 0 to 10%, the SSC susceptibility gradually increases. Presence of CO_2 reduces solution pH and facilitates the SSC process. As a consequence of CO_2 related corrosion, $FeCO_3$ scale is created on the surface. In presence of CO_2, H_2S corrosion process also results in formation of FeS scale, which augments the formation of protective layer that hinders the corrosion process.

c. Tested carbon steels displayed significant SSC susceptibility when CO_2 concentration is between 10 and 30%. Their PSF measurements show the existence of a critical CO_2 concentration at which the SSC susceptibility maximizes.

d. C-110 steel used in the investigation showed unexpected chemical composition trend when compared with other API steel grades. As resulted, it exhibited very low PSF, which indicates inherent lack of ductility. However, examining the dimensionless PSF, which shows the relative change of PSF

from the baseline, SSC susceptibility trend follows the anticipated nominal yield strength order: T-95 showed the highest SSC resistance while Q-125 display the least.

5.2 Recommendations

a. Influence of H_2S concentration should be evaluated by varying the H_2S partial pressure. Due to the environmental and safety regulation, H_2S concentration in this study was kept at approximately 300 ppm throughout the entire experiment.

b. Literatures state that temperature and total pressure are also critical parameters in determining SSC susceptibility. Impact of these parameters need to be studied to simulate wide ranges of sour environments.

c. Q-125 displayed substantial loss of ductility after exposure to brine and mixed gas containing 25% CO_2. Hence, further investigation is necessary to study the impact of CO_2 concentration on SSC resistance in this particular range of concentration (15% and 40%), in which severe decline in PSF was observed..

d. For yield strength and PSF calculation, 0.2% offset yield strength measurement is used in the study since the yield point is not easily defined from the experiment stress–strain curve. API recommends to use 0.5% offset method to mitigate the problems arising from 0.2% offset method by drawing a straight vertical line from 0.5% strain to the stress–strain curve and defining the yield strength as the stress value of the intersecting point. Hence, a mitigation procedure should be developed and implemented to scale the stress–strain curve in the elastic region to improve quality of measured data.

NOMENCLATURE

CERT	Constant Extension Rate Test
Cr	Chromium
DCB	Double Cantilever Beam
HRC	Rockwell Hardness
HV	Vickers Hardness
K_{ISSC}	Critical Stress Intensity Factor
Mo	Molybdenum
Ni	Nickel
P	Pressure (psi)
PSF	Plastic strain to failure
SCC	Stress Corrosion Cracking
SMYS	Specified Minimum Yield Strength (ksi)
SSC	Sulfide Stress Cracking
SSR	Slow Strain Rate
T	Temperature (°F)
UTS	Ultimate tensile strength
YS	Yield Strength

REFERENCES

API Specification 5CT, Specification for casing and tubing 9. 2005. Washington, DC: API.

Bell, T. 2016. Types of Corrosion. *The Balance*, January 29 2016, https://www.thebalance.com/types-of-corrosion-2340005 (accessed 5 December 2016).

Bourgoyne, A.T., Millheim, K.K., Chenevert, M.E. and Young, F.S. 1986. *Applied drilling engineering*, 1st ed. Richardson, Texas: The Society of Petroleum Engineers.

Bridgman, P. 1944. The stress distribution at the neck of a tension specimen. *Trans. ASM* **32**: 553-574.

Bridgman, P.W. 1952. *Studies in large plastic flow and fracture (Vol. 177)*. New York: McGraw-Hill.

Cernocky, E.P., Aaron, V.D., Paslay, P.R. and Wink, R.E. 2005. Combined axial tension/compression and internal pressure testing of mini-pipe specimens in H2S environment to determine three dimensional (triaxial) stress states which produce crack initiation failure: explanation of the new test fixture, mini-pipe specimen, and preliminary test results. Presented at SPE High Pressure/High Temperature Sour Well Design Applied Technology Workshop, Society of Petroleum Engineers, The Woodlands, Texas, 17-19 May. SPE-97577-MS. http://dx.doi.org/10.2118/97577-MS

Choudhary, B.K., Palaparti, D.R. and Samuel, E.I. 2013. Analysis of Tensile Stress-Strain and Work-Hardening Behavior in 9Cr-1Mo Ferritic Steel. *Metallurgical and Materials Transactions A* **44**(1): 212-223.

Ciaraldi, S.W. 1986. Some Factors That Affect the Sour-Service Performance of Carbon-Steel Oil-Country Tubulars. *SPE Drilling Engineering* **1**(03): 233-241. SPE-13844-PA. http://dx.doi.org/10.2118/13844-PA

Craig, B.D., Brownlee, J.K. and Bruno, T.V. 1992. Sulfide stress cracking of nickel steels. *Corrosion* **48**(2): 90-97. NACE-92020090.

Crowder, B., Buchanan, J., Mishael, S. and Shockley, R. 2011. Sulfide Stress Cracking Susceptibility of Local Hard Areas In Carbon Steel Weld Heat Affected Zones. Presented at CORROSION 2011, NACE International, Houston, Texas, 13-17 March. NACE-11105.

Dan, W.J., Zhang, W.G., Li, S.H. and Lin, Z.Q. 2007. An experimental investigation of large-strain tensile behavior of a metal sheet. *Materials & design* **28**(7): 2190-2196.

Davis, J.R. ed. 2004. *Tensile testing*, 2nd ed. Materials Park, Ohio: ASM international.

Elgaddafi, R., Ahmed, R., Hassani, S., Shah, S. and Osisanya, S.O. 2016. Corrosion of C110 carbon steel in high-pressure aqueous environment with mixed hydrocarbon and CO 2 gas. *Journal of Petroleum Science and Engineering* **146**: 777-787.

Elgaddafi, R., Ahmed, R. M. and Shah, S. N. 2016. Modeling CO2-H2S Corrosion of Tubular at Elevated Pressure and Temperature, *Research Journal of Applied Sciences, Engineering and Technology* **13**(7): 510-524.

Elgaddafi, R., Naidu, A., Ahmed, R., Shah, S., Hassani, S., Osisanya, S.O. and Saasen, A. 2015. Modeling and experimental study of CO2 corrosion on carbon steel at elevated pressure and temperature. *Journal of Natural Gas Science and Engineering* **27**: 1620-1629.

Garbatov, Y., Soares, C.G., Parunov, J. and Kodvanj, J. 2014. Tensile strength assessment of corroded small scale specimens. *Corrosion science* **85**: 296-303.

Hashizume, S. and Inohara, Y. 2000. Effects of pH and PH2S on SSC Resistance of Martensitic Stainless Steels, Presented at CORROSION 2000, NACE International, Orlando, Florida, 26-31 March. NACE-00130

Heidary, H., Refahi Oskouei, A. and Ahmadi, M. 2008. Mechanism detection of stress corrosion cracking by acoustic emission and effect of manufacturing process on AE signals. *Journal of the Acoustical Society of America* **123**(5): 3232.

Hibbeler, R. 2011. *Mechanics of Materials*, 8th ed. Upper Saddle River, NJ: Prentice Hall.

Hollomon, J.H. 1945. Tensile deformation. *AIME TRANS* **12**(4):1-22.

Hörstemeier, M., Bosch, C., Orlans, B. and Delattre, L. 2010. Validation Of The Constant Extension Rate Test (Cert) For High Strength OCTG Steels As A Ranking Tool For SSC Resistance. Presented at CORROSION 2010, NACE International, San Antonio, Texas, 14-18 March. NACE-10309.

Joun, M., Eom, J.G. and Lee, M.C. 2008. A new method for acquiring true stress–strain curves over a large range of strains using a tensile test and finite element method. *Mechanics of Materials* **40**(7): 586-593.

Kermani, M.B. and MacCuish, R.G. 1990. Materials Assessment for Sour Service Applications. Presented at SPE Annual Technical Conference and Exhibition, Society of Petroleum Engineers, New Orleans, Louisiana, 23-26 September. SPE-20457-MS. http://dx.doi.org/10.2118/20457-MS

Kimura, M., Kataoka, Y. and Nakano, Y. 1996. Sulfide stress corrosion cracking resistance of low Cr steel. Presented at CORROSION 96, NACE International, Denver, Colorado, 24-29 March. NACE-96060.

Koh, S.U., Kim, J.S., Yang, B.Y. and Kim, K.Y. 2004. Effect of line pipe steel microstructure on susceptibility to sulfide stress cracking. *Corrosion* **60**(3): 244-253. NACE-04030244.

Le Roy, G., Embury, J.D., Edwards, G. and Ashby, M.F. 1981. A model of ductile fracture based on the nucleation and growth of voids. *Acta Metallurgica* **29**(8): 1509-1522.

Ling, Y. 1996. Uniaxial true stress-strain after necking. *AMP Journal of Technology* **5**: 37-48.

Ludwik, P. 1909. Element der Technologischen. *Mechanik* p.32.

Misiolek, Z., Kowalczyk, J. and Kastner, P. 1977. Investigation of Plastic Flow Stresses of Zn and Its Alloys. *Arch. Hutn.* **22**(1): 71-88.

Morana, R. and Nice, P.I. 2009. Corrosion assessment of high strength carbon steel grades P-110, Q-125, 140 and 150 for H2S containing producing well environments. Presented at CORROSION 2009, NACE International, Atlanta, Georgia, 22-26 March. NACE-09093.

NACE MR0175/ISO 15156-2, Petroleum and Natural Gas Industries-Materials for Use in H2S-Containing Environments in Oil and Gas Production, Part 2: Cracking-Resistant Carbon and Low Alloy Steels, and the Use of Cast Irons. 2009. Houston, TX: NACE International.

NACE TM0198, Slow Strain Rate Test Method for Screening Corrosion-Resistant Alloys (CRAs) for Stress Corrosion Cracking in Sour Oilfield Service. 2004. Houston, TX: NACE International.

Papavinasam, S. 2013. The Main Environmental Factors Influencing Corrosion. In *Corrosion control in the oil and gas industry*, 1st ed, Chap. 4, 179-247. London: Elsevier.

Popoola, L.T., Grema, A.S., Latinwo, G.K., Gutti, B. and Balogun, A.S. 2013. Corrosion problems during oil and gas production and its mitigation. *International Journal of Industrial Chemistry* **4**(1): 1-15. http://dx.doi.org/10.1186/2228-5547-4-35

Poweleit, D. and Monroe, R. 2005. Steel Alloys. *Engineered Casting Solutions* **7**(2005): 24-28.

Ramberg, W. and Osgood, W.R. 1943. Description of stress-strain curves by three parameters. Technical note No. 90, NASA, Washington, DC (July 1943).

Rhodes, P.R., Skogsberg, L.A., Schofield, R., Kane, R.D. and Trillo, E.A. 2007. Evaluation Of Fitness-For-Purpose Test Environments For Sulfide Stress Cracking Tests Of Casing Steels. Presented at CORROSION 2007, NACE International, Nashville, Tennessee, 11-15 March. NACE-07112.

Srinivasan, S. and Kane, R.D. 1996. Prediction of corrosivity of CO2/H2S production environments. Presented at CORROSION 96, NACE International, Denver, Colorado, 24-29 March. NACE-96011.

Swift, H. 1952. Plastic instability under plane stress. *Journal of the Mechanics and Physics of Solids* **1**(1): 1-18.

Tale, S. 2014. *Sulfide Stress Cracking Behavior of Grade C-110 Steel Tubulars under High-pressure Conditions*. MS thesis, University of Oklahoma, Norman, Oklahoma.

Vera, J.R. and Case, R. 1997. The relationship between hydrogen permeation and sulfide stress cracking susceptibility of OCTG materials at different temperatures and pH values. Presented at CORROSION 97, NACE International, New Orleans, Louisiana, 9-14 March. NACE-97047.

Voce, E. 1948. The relationship between stress and strain for homogeneous deformation. *J Inst Met* **74**: 537-562.

Wang, Y.D., Xu, S.H., Ren, S.B. and Wang, H. 2016. An Experimental-Numerical Combined Method to Determine the True Constitutive Relation of Tensile Specimens after Necking. *Advances in Materials Science and Engineering* **2016**. 6015752. http://dx.doi.org/10.1155/2016/6015752

Zhano, K.S. and Li, Z.H. 1994. Numerical analysis of the stress-strain curve and fracture initiation for ductile material. *Engineering fracture mechanics* **49**(2): 235-241.

Zhigilei, L. V. 2010. Failure. Lecture notes MSE 2090: Introduction to Materials Science, University of Virginia, 7.